Infrared Spectroscopy of Matrix-Isolated Polycyclic Aromatic Compounds and their Ions. 6. Polycyclic Aromatic Nitrogen Heterocycles

A. L. Mattioda[1], Douglas M. Hudgins[1], C. W. Bauschlicher, Jr[1]., M.,Rosi[2], L. J. Allamandola[1]

1.-NASA Ames Research Center, MS 245-6, Moffett Field, CA 94035

2.-CNR Center for High Performance Computing in Molecular Sciences c/o Department of Chemistry, University of Perugia, 06123 Perugia, Italy

Submitted to: The Journal of Physical Chemistry, July xx, 2002

Suggested Running Title: Infrared Spectroscopy of PANHs

Keywords: Polycyclic aromatic compounds
Polycyclic aromatic nitrogen heterocycles
Fundamental vibrational frequencies
spectroscopy, infrared
Dipole moments
Rotational constants

ABSTRACT

The matrix-isolation technique has been employed to measure the mid-infrared spectra of several polycyclic aromatic nitrogen heterocycles in both neutral and cationic forms. The species studied include: 7,8 benzoquinoline ($C_{13}H_9N$); 2-azapyrene ($C_{15}H_9N$); 1- and 2- azabenz[a]anthracene ($C_{17}H_{11}N$); and 1-, 2-, and 4- azachrysene (also $C_{17}H_{11}N$). The experimentally measured band frequencies and intensities for each molecule are tabulated and compared with their theoretically calculated values computed using density functional theory at the B3LYP/4-31G level. The overall agreement between experiment and theory is quite good, in keeping with previous investigations involving the parent aromatic hydrocarbons. Several interesting spectroscopic trends are found to accompany nitrogen substitution into the aromatic framework of these compounds. First, for the neutral species, the nitrogen atom produces a significant increase in the total integrated infrared intensity across the 1600 - 1100 cm^{-1} region and plays an essential role in the molecular vibration that underlies an uncharacteristically intense, discrete feature that is observed near 1400 cm^{-1} in the spectra of 7,8 benzoquinoline, 1-azabenz[a]anthracene, and 4-azachrysene. The origin of this enhanced infrared activity and the nature of the new 1400 cm^{-1} vibrational mode are explored. Finally, in contrast to the parent hydrocarbon species, these aromatic nitrogen heterocycles possess a significant permanent dipole moment. Consequently, these dipole moments and the rotational constants are reported for these species in their neutral and ionized forms.

I. INTRODUCTION

Motivated in large part by their emerging importance in the field of astrophysics, the past decade has witnessed a renaissance in the study of the fundamental molecular and spectroscopic properties of polycyclic aromatic hydrocarbons (PAHs). Of particular interest has been the prominent and ubiquitous interstellar infrared emission signature that belies the presence of this class of compounds in a surprising variety of very disparate astronomical objects throughout our galaxy. [1] The drive to better understand the role of PAHs in the interstellar medium has catalyzed the establishment of comprehensive theoretical and experimental programs to study the fundamental spectroscopic characteristics of these species in both neutral and ionized forms. On the theoretical side, beginning with the work of Langhoff[2], the use of density functional theory (DFT) to calculate the harmonic frequencies and intensities of PAH species has revolutionized quantum chemical analyses of large molecular systems. This, coupled with rapid advances in computational power, has facilitated calculation of the infrared spectra of a wide range of PAHs[2,3,4], many of which are not accessible with current experimental techniques.[5] On the experimental side, the matrix isolation technique has been particularly prolific in providing the infrared absorption spectra of many PAH

species under conditions relevant to the astrophysical problem.[6,7,8] The theoretical calculations provide a valuable calibration of the magnitude of matrix effects in the experimental data while the experimental data provide a check for the effects of symmetry breaking which can seriously impact the accuracy of the theoretical calculations.[9]

In addition to the matrix experiments and DFT calculations, interest in molecular dynamics coupled with the critical data needs in the neighboring field of astrophysics have also driven the development of additional, elegant experimental techniques designed to explore the infrared properties of PAHs in the gas-phase. Using their SPIRES (Single Photo InfraRed Emission Spectroscopy) technique, Saykally and coworkers have directly measured the infrared emission spectra from several vibrationally excited, neutral and ionized PAHs in the gas phase under conditions identical to those of the interstellar emitters.[10] This work has yielded unique insight into the fundamental photophysics of infrared fluorescence in PAHs and PAH ions, the mechanism believed to drive the observed interstellar infrared emission and govern the interstellar UV/vis-to-IR conversion process. Working independently, Meijer and coworkers have pioneered a sensitive cluster-dissociation technique for directly measured the vibrational absorption spectrum of cold, gas-phase PAH cations in a free jet expansion using the tunable infrared beam of a free electron laser.[11] This work has revealed important details about the vibrational properties of isolated gas-phase PAH cations and provices a direct experimental measure of the matrix perturbations on the vibrational spectra of PAH ions. Overall, the agreement between the data provided by these latter techniques and those of the matrix experiments are surprisingly good. Together, these two new techniques provide further evidence supporting the interstellar PAH model and the utility of matrix isolation infrared absorption data for addressing the astrophysical problem.

The Astrochemistry laboratory at NASA Ames Research Center has an ongoing program to study the infrared spectroscopic properties of PAHs and PAH ions using a combination of experimental matrix-isolation measurements and theoretical DFT calculations. Previous papers in this series[8] have explored a variety of size and structural effects on the spectra of these species. These data are also available in electronic form on the internet at <http://www.astrochem.org/pahdata/index.html>. This paper explores the effects of incorporating a nitrogen atom in the aromatic network of several polycyclic aromatic species. For the first time the IR spectra of these polycyclic aromatic nitrogen heterocycles (alternatively PANHs; N-PAHs; or aza-PAHs) and includes the following species in both their neutral and ionized forms: 7,8 benzoquinoline ($C_{13}H_9N$), 2-azapyrene ($C_{15}H_9N$), 1- and 2- azabenz[a]anthracene, and 1-, 2-, and 4-azachrysene (all $C_{17}H_{11}N$) are presented. The structures of these species are shown in Figure 1.

This paper is laid out as follows. The experimental and theoretical methods are summarized in section II. The spectroscopic characteristics of PANH neutrals and PANH cations are presented

and discussed in sections III.a and III.b, respectively. The rotational parameters for the PANH species considered here are presented in section III.c. The paper is concluded with section IV.

II EXPERIMENTAL AND THEORETICAL METHODS

A. *Experimental.* The matrix isolation infrared spectroscopy techniques employed in these studies have been described in detail previously[8b,e] and will be summarized here only briefly. Matrix isolated PANH samples were prepared by vapor co-deposition of the species of interest with an over abundance of argon onto a 14K CsI window suspended in a high-vacuum chamber ($p < 10^{-8}$ mtorr). The PANH samples were vaporized from heated Pyrex tubes while argon was admitted through an adjacent length of $N_2(l)$-trapped copper tubing. Deposition temperatures for the PANHs studied were as follows: 7,8 benzoquinoline, room temperature; 2-azapyrene, 40°C; 1-azabenz[a]anthracene, 81°C; 2-azabenz[a]anthracene, 98°C; 1-azachrysene, 97°C; 2-azachrysene, 107°C; 4-azachrysene, 104°C, and. Due to their relatively high volatilities, 2-azapryene and 7,8-benzoquinoline were deposited through a short length of heated copper tubing fitted with a valve (Whitey model #SS-8BK). The valve was opened to admit the PANH vapor during deposition, but otherwise was kept closed to prevent a continuous flow of this vapor into the sample chamber throughout the experiment. Estimates based on the characteristic band intensities of PAHs and the calibrated argon deposition rate place the Ar/PANH ratio in these experiments in excess of 1000/1.[8e] 7,8-benzoquinoline (98+%) was obtained from Sigma/Aldrich Chemical Co. The remaining PANH samples used in these experiments were obtained from the National Cancer Institute's Chemical Carcinogen Reference Standard Repository operated by the Midwest Research Institute. All samples are of unspecified purity, however the absence any notable discrepant spectral features between the theoretical and experimental spectra indicate impurity levels are no more than a few percent.

Spectra from 6000 - 500 cm^{-1} were measured on either a Nicolet 740 or a Digilab Excalibur FTS 4000 FTIR spectrometer using a KBr beamsplitter and $N_2(l)$-cooled MCT detector. Each spectrum represents a coaddition of between 500 and 1024 scans at a resolution of 0.5 cm^{-1}. This level of resolution is critical for detecting ion bands which fall near the position of a neutral band, while the number of scans was chosen to optimize both the signal-to-noise as well as time requirements of each experiment. Integrated intensities ($\int \tau \, d\tilde{\nu}$) for individual bands were determined using the WIN IR Pro spectrometer control/data analysis software package provided by Digilab. Absolute intensities ($A \equiv \int \tau \, d\tilde{\nu} \Big/ N$, where N is the surface density of absorbers in molecules/cm^2) for the experimentally measured neutral PANH bands were determined using the

theoretically calculated values as follows. The theoretically calculated intensities for all bands between 1600 and 500 cm^{-1} were summed to obtain the total absorption intensity over this region. This range was chosen to exclude the contributions of the far infrared bands ($\tilde{\nu} < 500\ cm^{-1}$) that were not measured in the experiments and those of the CH stretching bands which blend with overtone/combination bands in the experimental data and whose intensities are substantially overestimated by the calculations.[3a,8e] The total theoretically calculated absolute intensity was then distributed over the experimental bands on the basis of the fractional contribution of each to the total 1600 to 500 cm^{-1} absorption in the experimental spectrum:

$$A_i^{exp.} = \left[\sum_{1600 \geq \tilde{\nu} \geq 500} A^{thy.} \right] \bullet \frac{I_{rel,i}^{exp.}}{\sum_{1600 \geq \tilde{\nu} \geq 500} I_{rel}^{exp.}}$$

This method takes advantage of the fact that, while there may be significant band-to-band variability in the accuracy of the calculated intensity, the total intensity is expected to be quite accurate.

PANH cations were generated by *in-situ* vacuum ultraviolet photolysis of the matrix isolated neutral PANH. This was accomplished with the combined 120 nm Lyman-α/160 nm molecular hydrogen emission bands (10.1 and 7.77 eV, respectively) from a microwave powered flowing H_2 discharge lamp at a dynamic pressure of 150 mTorr. Comparison of the pre-photolysis neutral spectrum to that measured after photolysis permitted identification of PANH ion features.[8h] To confirm the attribution of a photoproduct band to a particular PANH cation, parallel experiments were conducted in which the argon matrix was doped with an electron acceptor, NO_2 and in some instances CCl_4, at a concentration of approximately 1 part in 1000. The presence of this electron acceptor quenches the formation of PANH anions and enhances the production of cations. For a particular photoproduct band to be assigned to the PANH cation, it must grow in the presence of the electron acceptor and do so in fixed proportion to the other bands attributed to the cation.

Assuming that all neutral PANHs which disappear upon photolysis are converted into cations, we can derive an upper limit to the ionization efficiency by measuring the percent decrease in the integrated areas of the neutral bands that accompany photolysis. The upper limits for the spectra reported here were: 7,8-benzoquinoline, 11% (in presence of NO_2); 2-azapyrene, 11%; 1-azabenz[a]anthracene, 3%; 2-azabenz[a]anthracene, 10%; 1-azachrysene, 7%; 2-azachrysene, 13%; and 4-azachrysene, 5%. Due to experimental difficulties, the results reported for 7,8 benzoquinoline are those of an Ar/NO_2 electron acceptor experiment instead of the typical neat Ar experiment No significant anion formation was observed in any of the compounds discussed in this publication.

B. *Theoretical.* For the species treated here, the geometries are optimized and the harmonic frequencies computed using density functional theory (DFT). Specifically, the hybrid[12] B3LYP[13]

functional was utilized in conjunction with the 4-31G basis sets.[14] Calibration calculations[3a], which have been carried out for selected systems, show that a single scale factor of 0.958 brings the B3LYP harmonic frequencies computed using the 4-31G basis set into excellent agreement with the experimental fundamental frequencies. For example, for neutral 1-azachrysene the average absolute discrepancy is 5.4 cm^{-1} and the maximum error is 14.9 cm^{-1}. While the error can be reduced by increasing the basis set (provided the C-H stretches are scaled separately), the B3LYP/4-31G results are of sufficient accuracy to allow a critical evaluation of experiment. The calibration calculations also show that the computed B3LYP/4-31G intensities are accurate except for C-H stretches which are, on average, about a factor of two larger than those determined in the matrix studies.[3a,8e] While the gas-phase data are very limited, it appears that the gas-phase intensities tend to lie between the matrix and B3LYP values.[10,11] It has also been observed that when two bands of the same symmetry are close in energy, their relative intensities are sensitive to the level of theory, but the sum of their intensities is very reliable.

In contrast to their hydrocarbon counterparts, the PANHs studied here all have significant permanent dipole moments and therefore exhibit pure rotational spectra. Although the rotational spectra are not measured experimentally in this study, the relevant rotational constants and dipole moments have been calculated from the Gaussian output. The B3LYP dipole moments are computed at the center of mass, with the x, y, and z axes aligned along the principle moments of inertia. The rotational constants are computed using the equilibrium B3LYP geometry, with vibrational contributions to the geometry neglected.

All calculations were performed using the Gaussian 98 computer code.[15] . The net charge on each atom is determined using the Mulliken population analysis. To aid in the analysis, the vibrational modes and displacement vectors are viewed using the interactive molecular graphics tool MOLEKEL.[16]

III. RESULTS

A. *The 4000 to 500 cm^{-1} spectra of neutral PANHs.* The measured mid-infrared spectra of the argon matrix isolated PANHs considered in this study are presented according to family. Figure 2 shows the spectra of 1-, 2-, and 4-azachrysene. Figure 3 shows the spectra of 1-, and 2-azabenz[a]anthracene. Figures 4 and 5 show the spectra of 2-azapyrene and 7,8-benzoquinoline, respectively. -The spectrum of the corresponding parent hydrocarbon of each family is included in each case for reference. The observed band positions and intensities are tabulated and compared to their theoretically calculated values grouped in analogous fashion with the azachrysenes in Table 1, the azabenz[a]anthracenes in Table 2, and 7,8-benzoquinoline and 2-azapyrene in Table 3.

Close inspection of Tables 1-3 shows that, as with most PAHs previously studied, the agreement between the measured peak positions and their theoretically calculated counterparts is generally good. Most measured bands lie within 5 to 10 cm^{-1} of predicted values, some within 20 cm^{-1} and only a few differ by as much as 30 cm^{-1}. However, the variation between the measured and calculated band intensities are significantly larger, with differences of factors of three or more common. In spite of this, the overall agreement between theory and experiment is reasonable, and the calculated normal modes, charge distributions, dipole moments, etc. provide valuable insight into the molecular characteristics.

In principle, nitrogen substitution in the carbon skeleton of an aromatic compound introduces three new categories of vibrational modes--aromatic CN stretching, and CNC in-plane bending and out-of-plane warping modes, the latter of which fall primarily in the far-infrared region below 500 cm^{-1}. These N-involved vibrations cannot, however, operate independently from the rest of the molecule. Instead, they mix to varying degrees with other CC and CH modes of the same symmetry and similar energy to produce the normal modes of the molecule. Consequently, it is difficult, if not impossible, to identify specific features in the mid-infrared spectra of PANHs that can be unambiguously attributed to vibrations involving the nitrogen atom. Instead, it is more precise to speak in terms of *nitrogen-dominated* modes—modes to which motion of the nitrogen atom contributes a disproportionately large fraction of the infrared activity. These contributions have been quantified through analysis of the individual atomic displacements associated with each vibrational mode in the Gaussian output.

In general, nitrogen-dominated modes will fall at lower frequencies than the analogous pure carbon modes of aromatic hydrocarbons, due to the larger mass of the N atom. Nevertheless, despite this shift, inspection of Figures 2-5 shows that, in the neutral species, nitrogen substitution is not accompanied by the appearance of any prominent bands in regions of the spectrum that would clearly distinguish them from the modes of the parent aromatic hydrocarbons. Consequently, it is not possible to distinguish the nitrogen-dominated vibrational modes of PANHs on the basis of the experimental data alone. Turning to theoretical data, decomposition of the individual atomic displacements of the calculated vibrations reveals that modes dominated by CN stretching and CNC in-plane bending tend to fall in the 1100-1000 cm^{-1} region. Indeed, close inspection of Figures 2-5 does reveal a general increase in infrared activity in this region for the PANHs compared to their parent PAH. These modes are, however, weak to very weak ($I_{rel} \leq 0.1$) and are not even included in Tables 1-3. This explains the failure of these modes to produce a notable impact on the appearance of the observed spectra. As mentioned previously, the out-of-plane CNC warping modes make their greatest contributions to the lowest frequency modes of the molecule. Although many of these fall in the far-infrared region of the spectrum, several modes in

the 600 - 500 cm^{-1} region have been found to carry significant CNC out-of-plane warping character as well.

Despite the global similarity between the spectra of the neutral PANHs and those of their parent PAHs, there are two aspects of the spectra shown in Figures 2-5 that set the spectra of nitrogen-bearing aromatics apart. First, inspection of these figures shows that nitrogen addition induces a pronounced, global enhancement of the features in the region between 1650 and 1100 cm^{-1}, reminiscent of the spectral change that accompanies ionization.[7a,8a] This behavior is quantified in Table 4 which shows the integrated intensity across the 1600 to 1100 cm^{-1} region, as well as the integrated intensities across the 1100 to 500 and 3100 to 3000 cm^{-1} regions, for each of the species in Figures 2-5. The modes that fall in the 1600 to 1100 cm^{-1} region correspond to the aromatic CC and CN stretching and CH in-plane bending vibrations. For the PANH species, the total absorption intensity is twice that of the corresponding PAH. For 2-azapyrene (C_{2v} symmetry), 7,8-benzoquinoline, and the three azachrysenes (all C_s symmetry) this may, in part, be due to a general increase in the number of infrared active modes resulting from the lower symmetry of the PANH species compared to the parent PAHs (pyrene, D_{2h}; phenanthrene, C_{2v}, chrysene, C_{2h}). However, this effect is also observed in the azabenz[a]anthracenes (C_s symmetry) which share the same symmetry as their parent PAH, so this effect cannot be solely attributed to lowering of the molecular symmetry.

Table 4 also shows that, for the neutral species, nitrogen insertion does not substantially alter the total absorption intensity of the CH out-of-plane bending and skeletal deformation modes in the 1100 to 500 cm^{-1} region. However, the CH stretching modes in the 3100 to 3000 cm^{-1} are mildly suppressed by approximately 25%. These effects are also similar to that found to accompany ionization, although the enhancement of the CC stretching/CH in-plane bending modes and the suppression of the CH stretching modes is more modest than that which accompanies ionization. Together, these observations suggest that substitution of the electronegative nitrogen atom in the aromatic network of the PANHs produces a pseudo-ionization effect. Indeed, this hypothesis is supported by an analysis of the average Mulliken populations on the carbon atoms of the PANHs and their parent PAHs listed in Table 5. In all cases, nitrogen insertion modifies the average charge on each carbon atom to the point that it more closely resembles the charge on the carbon atoms of the parent PAH *cation* than that of the the parent neutral PAH. Hence, the observed pseudo-cationic nature of the mid-infrared spectra.

The second unique influence of nitrogen substitution on the infrared spectra of neutral PANHs is the appearance of a significant new band near 1400 cm^{-1} for 1-azabenz[a]anthracene, 4-azachrysene, and 7,8 benzoquinoline. This feature is marked with an arrow in Figures 2, 3, and 5.

In each of the species showing this feature, the nitrogen is para to a CH group. The vibrational motion that gives rise to this uncharacteristically strong feature is illustrated for 7,8-benzoquinoline in Figure 6. The mode is dominated by a rocking of the CNC bond combined with a exaggerated in-plane wagging of the para CH group. Only one of the molecules considered in this study, 1-azachrysene, shares this structural characteristic but does not show an unusually intense feature in the vicinity of 1400 cm^{-1}. Analysis of the atomic displacements in for this mode in the Gaussian output shows that in this molecule, out of phase CH in-plane motions elsewhere in the molecule effectively quench the intensity of the mode.

B. *The 4000 to 500 cm^{-1} spectra of PANH cations.* The spectra of the argon matrix isolated 1-azachrysene, 2-azachrysene, and 4-azachrysene cations are compared to that of the parent chrysene cation in Figure 7. Likewise, the spectra of the 1-azabenz[a]anthracene and 2-azabenz[a]anthrecene cations are compared to the benz[a]anthracene cation in Figure 8; the spectrum of the 2-azapyrene cation is compared to that of the pyrene cation in Figure 9; and the spectrum of the 7,8-benzoquinoline cation is compared to that of the phenanthrene cation in Figure 10. The observed band positions and relative intensities of the azachrysene cations, the azabenz[a]anthracene cations, the 2-azapyrene cation, and the 7,8-benzoquinomline cation are tabulated and compared to their theoretically calculated values in Tables 6, 7, and 8, respectively. For the ions, due to uncertainties in establishing ion concentration and charge effects within the matrix, only relative band intensities are reported for the experiments.

Inspection of Tables 6-8 reveals frequency discrepancies between theory and experiment that are somewhat higher than for the neutral species described above. For the cations, although the positional agreement between theory and experiment is similar to or only slightly poorer that that observed for the neutral species, more striking is the substantially larger number of bands predicted by theory than are observed in the experimental data. The most probable explanation for the lower-than-expected number of observed cation bands is the pseudo-ionization effect discussed in the previous section. Given that neutral PANH molecules exhibit some of the spectroscopic character of ionized species, it is likely that the average band position shift induced by ionization is less than that observed for the aromatic hydrocarbon cations studied previously. Since photolysis of a neutral sample even under the best of conditions converts only ca. 10% of the precursor neutral species into cations, screening of cation bands by residual neutral bands in the post-photolysis spectra represents a relatively greater problem for the PANH species considered here. For example, consider the CH out of plane bending features of the 4-azachrysene cation observed at 777.3, and 754.4 cm^{-1} (theory: 781.5, and 758.9 cm^{-1}). These positions are nearly identical to the corresponding features of the neutral molecule visible at 778.1, and 753.2 cm^{-1} (theory: 781.5, and 755.5 cm-1). Indeed, these cation features are completely subsumed by their stronger, neutral

counterparts in the post-photolysis spectrum and are observable in the difference spectrum (Figure 7) only by virtue of their intrinsic strength. For weaker bands this will not be the case, and it is likely that a high proportion of these bands are not observable in the experimental data. This is particularly true for the CH stretching region between 3100 and 3000 cm^{-1} where, as has been the case with previous IR studies of positively charged aromatic molecules, the strongly suppressed cation bands cannot be differentiated from the strong bands of the parent neutral. Again, relative intensity differences are greater than those associated with the band positions, with differences of a factor of 2 being common and some considerably higher.

Overall, the effects of ionization on the infrared spectra of PANHs are similar to those observed previously for PAHs. These effects are quantified in Table 9 which compares the total theoretically-calculated absorption intensities in the 1100 - 500 cm^{-1}, 1600 - 1100 cm^{-1}, and 3150 - 2950 cm^{-1} regions for PANHs in their neutral and cationic forms. The analogous experimental data is not shown due to the incomplete coverage of these features in that data as discussed above. For the bands in the 3150 - 2950 cm^{-1} region, the effect of ionization on the PANH spectra is identical to that observed for the analogous PAHs and involves a suppression by nearly an order of magnitude. Summing the intensities of the bands in the 1100 - 500 cm^{-1} region we find a modest but significant 40% enhancement of the total absorption intensity in this region. This result would seem to be at odds with our previous reports that the strongest CH out-of-plane bending modes of PAHs are modestly *suppressed* by ionization.[8b,c,d,h] However, those earlier reports focused individually on only the strongest bands in this region, not the composite behavior of all the bands in the region. Indeed, employing the analogous analysis,[8b] the experimental PANH data do indicate that, ionization produces a suppression of the individual PANH CH out-of-plane bands entirely consistent with that noted previously for the parent aromatic hydrocarbons. Clearly, there is sufficient enhancement in the other modes that fall in this region of the mid-infrared (e.g. skeletal distortion modes) that, taken as a group, the total integrated intensity increases. For comparison, the theoretical calculations indicate that the individual CH out-of-plane modes in PANHs are, on average, virtually unchanged by ionization. Thus, these data are also in agreement that the observed global enhancement of the intensity in the 1100 - 500 cm^{-1} region arises from modes other than the dominant CH out-of-plane bends.

Although the 1600 - 1100 cm^{-1} modes in PANHs are strongly enhanced by ionization, that enhancement is roughly half that observed for the analogous PAHs. This is understandable in terms of the pseudo-ionization effect that substitution of the electronegative nitrogen atom into the carbon skeleton has on these modes (see §III.A)--the charge distribution on the carbon skeleton of a neutral PANH is already intermediate between that of a neutral PAH and that of its (the PANH's)

cation; consequently, the magnitude of the ionization effect is somewhat attenuated. Taking all of the above into account, the total absorption intensities of the PANH cations do not differ significantly from that of the analogous PAH cations.

In the previous section, it was noted that the higher electronegativity of the nitrogen atom decreases the electron density surrounding the carbon atoms in the neutral PANH, creating the pseudo-ionization effect and enhancing CC and CH modes. It is natural to expect that the formation of a PANH cation, which would lower the electron density surrounding the nitrogen atom, would significantly enhance the nitrogen-dominated modes. Indeed, according to the Gaussian results, modes exhibiting appreciable amounts of nitrogen motion exhibit enhancements analogous to those observed in the CC stretching and CH in-plane bending modes. The characteristic regions for the nitrogen dominated modes are similar to those observed for the neutral species: 1100-1000 cm^{-1} for modes involving significant CN stretching or CNC in-plane bending; 600-500 cm^{-1} and below for modes involving significant CNC out-of-plane warping.

C. PANH Dipole Moments. By virtue of their permanent dipole moments, PANHs will exhibit pure rotational spectra making them potentially attractive candidates for an astronomical search. In view of this potential, the rotational constants and dipole moments for the species studied here have also been calculated using the Gaussian output. The components of the dipole moment along each of the molecules' rotational axes and the rotational constants about each of these axes are summarized in Table 10. Previous studies of the benzene molecule indicate that these quantities are likely accurate to within 1%.

All the PANH species considered in this study are asymmetric top molecules (i.e. the moments of inertia about each of the molecule's three internal coordinate axes is different). The rotational axes of each molecule are identified as a, b, and c on the basis of the moment of inertia, I, about each axis and according to the convention $I_a < I_b < I_c$. The rotational constants about the a, b, and c axes are denoted A, B, and C, respectively and are determined by the standard expression:

$$Q = \frac{\hbar}{4\pi c I_q}$$

where Q (= A, B, or C) is the rotational constant and I_q is the moment of inertia about the q axis. These rotational constants correspond to rotational transitions that fall in the centimeter-wavelength range of the radio region of the electromagnetic spectrum.

The B3LYP dipole moments are computed at the center of mass of each molecule, with the x (horizontal), y (vertical), and z (normal to the plane of the figure) axes aligned along the principle moments of inertia. The magnitude and direction of these dipole moments are indicated by the arrows next to each structure in Figure 1. Arrows for both the neutral (black) and cationic (gray) forms of each species are included in the diagram and the arrows point from negative to positive end

of the associated dipole. Perusal of Figure 1 and Table 10 shows that, on average, PANHs all possess substantial dipole moments with those of ionized PANHs being somewhat larger than neutral PANHs. Neutral PANHs have dipole moments which range from 1.67 to 3.37 Debye while the values for positively charged PANHs lie between 2.24 and 5.44 Debye. For these planar species, the components of these dipole moments are necessarily confined to the plane of the molecule, as observed in Table 10 ($\mu_c \equiv 0$ in all cases). For reference, the dipole moments for CO, H_2CO, and HC_3N are 0.117, 2.34, and 3.6 Debye respectively.

V. CONCLUSIONS

The mid-infrared spectra of the argon matrix isolated, N-containing aromatic compounds 7,8 benzoquinoline ($C_{13}H_9N$), 2-azapyrene ($C_{15}H_9N$), 1- and 2- azabenz[a]anthracene ($C_{17}H_{11}N$), and 1-, 2-, and 4-azachrysene (also $C_{17}H_{11}N$) in their neutral and cation forms are reported. Comparisons between these spectra and spectra computed using density functional theory at the B3LYP/4-31G level is quite good, consistent with earlier comparisons on homonuclear polycyclic aromatic hydrocarbons.

Nitrogen insertion induces several new spectroscopic trends for the aromatic family of molecules. For the neutral species, nitrogen inclusion causes unusual intensity enhancements for bands between 1600 and 1100 cm^{-1}, the CC stretching and CH in-plane bending vibrations, and induces new IR activity near 1400 cm^{-1}, corresponding to a mode which is characteristic of a particular N substitution site. Upon ionization, the spectral effects are similar to those reported previously for the corresponding aromatic hydrocarbon species. Although the CN, CC, and CH vibrational motions are heavily mixed in the vibrational modes of the neutral and cationic PANH species considered in this study, several modes in the 1100-1000 cm^{-1} region were found to carry significant contributions from CN stretching and CNC in-plane bending while several modes in the 600-500 cm^{-1} region were found to carry significant contributions from CNC out-of-plane warping motions.

Calculated dipole moments and rotational constants are also presented for both the neutral and cationic states of these polar, asymmetric top species. The rotational parameters for the PANHs studied here indicate that these species will exhibit centimeter-wavelength pure rotational spectra in the radio region of the electromagnetic spectrum.

VI. ACKNOWLEDGEMENTS

This project was performed, in part, using compounds provided by the National Cancer Institute's Chemical Carcinogen Reference Standards Repository operated under contract by Midwest Research Institute, No. N02-CB-07008. The authors also wish to acknowledge the expert

technical support of Bob Walker. Dr. Mattioda gratefully acknowledges the support of the National Research Council's Research Associateship Program. Dr. M. Rosi thanks the CNR for a short-term fellowship. This work was fully supported by NASA's Laboratory Astrophysics and Long Term Space Astrophysics programs, under grants #188-44-57-01 and # 399-20-01-05.

FIGURE CAPTIONS

Figure 1. The structures of the PANH species considered in this study. Small open circles represent hydrogen atoms; large open circles represent carbon atoms. The large filled circle represents the nitrogen atom in each structure. The "**x**" in each structure indicates the location of the center of mass of the molecule. The arrows to the right of each structure indicate the magnitude and orientation of the calculated dipole moment for each molecule. In each case, the black arrow represents the dipole moment of the neutral species while the gray arrow represents the dipole moment of the cation. The "a" rotational axis is horizontal, the "b" rotational axis is vertical, and the "c" rotational axis is normal to the plane of the figure.

Figure 2. The mid-infrared spectra of 1-, 2-, and 4-azachrysene isolated in an argon matrices. The spectrum of the parent hydrocarbon, chrysene, is shown for reference. All matrices were deposited and measured at 14K. The argon to PANH/PAH ratio was in excess of 1200/1. The arrow indicates the feature discussed in § III.a. An asterisk (*) indicates the position of a contaminant band (primarily H_2O).

Figure 3. The mid-infrared spectra of 1- and 2-azabenz[a]anthracene isolated in an argon matrices. The spectrum of the parent hydrocarbon, benz[a]anthracene, is shown for reference. All matrices were deposited and measured at 14K. The argon to PANH/PAH ratio was in excess of 1200/1. The arrow indicates the feature discussed in § III.a. An asterisk (*) indicates the position of a contaminant band (primarily H_2O).

Figure 4. The mid-infrared spectrum of 2-azapyrene isolated in an argon matrix. The spectrum of the parent hydrocarbon, pyrene, is shown for reference. All matrices were deposited and measured at 14K. The argon to PANH/PAH ratio was in excess of 1200/1. An asterisk (*) indicates the position of a contaminant band (primarily H_2O).

Figure 5. The mid-infrared spectrum of 7,8-benzoquinoline isolated in an argon matrix. The spectrum of the parent hydrocarbon, phenanthrene, is shown for reference. All matrices were deposited and measured at 14K. The argon to PANH/PAH ratio was in excess of 1200/1. The

argon to PANH/PAH ratio was in excess of 1200/1. An asterisk (*) indicates the position of a contaminant band (primarily H_2O).

Figure 6. The relative atomic displacements contributing to the nominal "1400 cm^{-1}" vibrational mode in 7,8-benzoquinoline.

Figure 7. The mid-infrared spectra of the 1-, 2-, and 4-azachrysene cations isolated in argon matrices at 14K. The spectrum of the chrysene cation is shown for reference. The spectra are the difference between the spectra of the argon matrix-isolated samples measured before and after Lyman-α photolysis. The bands marked by an asterisk (*) are contaminant photoproducts.

Figure 8. The mid-infrared spectra of the 1- and 2-azabenz[a]anthracene cations isolated in argon matrices at 14K. The spectrum of the benz[a]anthracene cation is shown for reference. The spectra are the difference between the spectra of samples in measured before and after *in-situ* Ly-α photolysis. Due to experimental difficulties, the 2-azabenz[a]anthracene spectrum is a combination of data from two experiments. The 1600-1000 cm^{-1} portion of the spectrum is taken from a neat argon matrix-isolated sample while the 1000-700 cm^{-1} portion is taken from a sample in which the argon matrix was doped with the electron acceptor NO_2 (Ar/NO_2~1000/1). The two spectra were scaled to compensate for differences in the ion yields of the two experiments. The bands marked by an asterisk (*) are contaminant photoproducts.

Figure 9. The mid-infrared spectra of the 2-azapyrene cation isolated in an argon matrix at 14K. The spectrum of the pyrene cation is shown for reference. The spectra are the difference between the spectra of the argon matrix-isolated samples measured before and after Lyman-α photolysis. The bands marked by an asterisk (*) are contaminant photoproducts.

Figure 10. The mid-infrared spectra of the 7,8-benzoquinoline cation isolated in an argon matrix at 14K. The spectrum of the phenanthrene cation is shown for reference. These spectra are the difference between the spectra of samples measured before and after *in-situ* Ly-α photolysis. Due to experimental difficulties, the 7,8-benzoquinoline cation spectrum is a combination of data

from two experiments. The 1600-1000 cm^{-1} portion of the spectrum is taken from a sample in which the argon matrix was doped with 1 part in 1000 of CCl_4 while the 1000-700 cm^{-1} portion is taken from a sample in which the argon matrix was doped with 1 part in 1000 of NO_2. The two spectra were scaled to compensate for differences in the ion yields of the two experiments. The bands marked by an asterisk (*) are argon photolysis products.

REFERENCES

1 Cox, P. and Kessler, M.F. *The Universe as Seen by ISO, Vol 2, ESA SP-427.* ESTEC, ESA Publications Division; Noordwijk, The Netherlands, 1999.

2 Langhoff, S.R. (1996) *J.Phys.Chem.*, **100**, 2819.

3 (a) Bauschlicher, C.W., and Langhoff, S.R. (1997) *Spectrochim.Acta A*, **53**, 1225; (b) Bauschlicher, C.W., Jr., Langhoff, S.R., Sandford, S.A., and Hudgins, D.M. (1997) *J.Phys.Chem.A*, **101**, 2414; (c) Langhoff, S.R. Bauschlicher, C.W., Jr., Hudgins, D.M., Sandford, S.A., and Allamandola, L.J. (1998) *J.Phys.Chem.A*, **102**, 1632; (d) Bauschlicher, C.W. (1998) *Chem.Phys.*, **233**, 29 (e) Bauschlicher, C.W., and Langhoff, S.R. (1998) *Chem.Phys.*, **234**, 79; (f) Bauschlicher, C.W., (1998) *Chem.Phys.*, **234**, 87; (g) Bauschlicher, C.W. (1998) *Chem.Phys.*, **234**, 87; (h) Bauschlicher, C.W., and Bakes, E.L.O. (2000) *Chem.Phys.*, **262**, 285.

4 (a) Talbi, D., Pauzat, F., Ellinger, Y. (1993) *Astron.Astrophys.*, **268**, 805; (b) de Frees, D.J., Miller, M.D., Talbi, D., Pauzat, F., and Ellinger Y. (1993) *Ap.J.*, **408**, 530; (c) Pauzat, F., Talbi, D., and Ellinger, Y. (1995) *Astron.Astrophys.*, **293**, 263; (d) Pauzat, F., Talbi, D., and Ellinger, Y. (1999) *MNRAS*, **304**, 241; (e) Pauzat, F., and Ellinger, Y. (2001) *MNRAS*, **324**, 355.

5 e.g. (a) Pauzat, F., Talbi, D., and Ellinger, Y. (1997) *Astron.Astrophys.*, **319**, 318; (b) Hudgins, D.M., Bauschlicher, C.W., and Allamandola, L.J. (2001) *Spectrochim.Acta.A*, **57**, 907.

6 Halasinski, T., Hudgins, D.M., Salama, F., Allamandola, L.J., and Bally, T. (2000) *J.Phys.Chem.*, **104**, 7484.

7 (a) Szczepanski, J., Roser, D., Personette, W., Eyring, M., Pellow, R., and Vala, M. (1992) *J.Phys.Chem.*, **96**, 7876; (b) Szczepanski, J., and M. Vala (1993) *Nature* **363**, 699; (c) Szczepanski, J., and Vala, M. (1993) *Ap.J.*, **414**, 179; (d) Szczepanski, J., Chaabo, C., and Vala, M. (1993) *Chem Phys*, **205**, 434; (e) Szczepanski, J., Vala, M., Talbi, D., Parisel, O., Ellinger Y.J. (1993) *J.Chem.Phys.*, **98**, 4494; (f) Vala, M., Szczepanski, J., Pauzat, F., Parisel, O., Talbi, D, and Ellinger, Y.J. (1994) *J.PhysChem.*, **98**, 9187; (g) Szczepanski, J., Wehlburg, C., and Vala, M. (1995) *Chem.Phys.Lett.*, **232**, 221; (h) Szczepanski, J., Drawdy, J., Wehlburg, C., Vala, M. (1995) *Chem.Phys.Lett.*, **245**, 539.

8 (a) Hudgins, D., Sandford, S.A., and Allamandola, L.J. (1994) *J.Phys.Chem.*, **98**, 4243; (b) Hudgins, D.M., and Allamandola, L.J. (1995) *J.Phys.Chem.*, **99**, 3033; (c) Hudgins, D.M., and Allamandola, L.J. (1995) *J.Phys.Chem.*, **99**, 8978; (d) Hudgins, D.M., and Allamandola, L.J. (1997) *J.Phys.Chem.*, **101**, 3472; (e) Hudgins, D.M., and Sandford, S.A (1998) *J.Phys.Chem.A*, **102**, 329; (f) Hudgins, D.M., and Sandford, S.A.

(1998) *J.Phys.Chem.A*, **102,** 344 (g) Hudgins, D.M., and Sandford, S.A. (1998) *J.Phys.Chem.A*, **102,** 353; (h) Hudgins, D.M., Bauschlicher, C.W., Jr., Allamandola, L.J., and Fetzer, J.C. (2000) *J.Phys.Chem.A*, **104**, 3655.

9 Bauschlicher, C.W., Jr., Hudgins, D.M., and Allamandola, L.J. (1999) *Theor.Chem.Acc.*, **103**, 154.

10 (a) Schlemmer, S., Cook, D.J., Harrison, J.A., Wurfel, B., Chapman, W., and Saykally, R.J. (1994) *Science*, **265**, 1686; (b) Cook, D.J., and Saykally, R.J. (1998) *Ap.J.*, **493**, 793; (c) Wagner, D.R., Kim, H.-S., and Saykally, R.J. (2000) *Ap.J.*, **545**, 854; (d) Kim, H.-S., Wagner, D.R., and Saykally, R.J. *Ap.J.*, (in press, 2001).

11 (a) Piest, J.A., von Helden, G. and Meijer, G. (1999) *Ap.J.* **520**, L75; (b) Piest, J.A., Oomens, J., Bakker, J., von Helden, G., and Meijer, G. (2001) *Spectrochim.Acta A*, **57A**, 717.

12 Becke, A.D. *J.Chem.Phys.*, **1993**, *98,* 5648.

13 Stephens, P.J.; Devlin, F.J.; Chabalowski, C.F.; Frisch, M.J., *J.Phys.Chem.*, **1994**, *98*, 11623.

14 Frisch, M.J.; Pople, J.A.; Binkley, J.S., *J.Chem.Phys.*, **1984**, *80*, 3265 and references therein.

15 GAUSSIAN 94, Revision D.1 Frisch, M.J., Trucks, G.W., Schlegel, H.B., Gill, P.M.W., Johnson, B.G., Robb, M.A., Cheeseman, J.R., Keith, T., Petersson, G.A., Montgomery, J.A., Raghavachari, K., Al-Laham, M.A., Zakrzewski, V.G., Ortiz, J.V., Foresman, J.B., Cioslowski, J., Stefanov, B.B., Nanayakkara, A., Challacombe, M., Peng, C.Y., Ayala, P.Y., Chen, W., Wong, M.W., Andres, J.L., Replogle, E.S., Gomperts, R., Martin, R.L., Fox, D.J., Binkley, J.S., Defrees, D.J., Baker, J., Stewart, J.P., Head-Gordon, M., Gonzalez, C., and Pople, J.A., GAUSSIAN, Inc., Pittsburgh PA, 1995.

16 MOLEKEL 4.2, P. Flükiger, H.P. Lüthi, S. Portmann, J. Weber, Swiss Center for Scientic Computing, Manno (Switzerland), 2000-2002. Stefan Portmann & Hans Peter Lüthi. MOLEKEL: An Interactive Molecular Graphics Tool. *CHIMIA* (2000) **54** 766-770.)

Table 1. Theoretical and experimental band positions and intensities for the neutral azachrysenes.[a]

1-azachrysene							2-azachrysene							4-azachrysene						
THEORY				EXPERIMENT			THEORY				EXPERIMENT			THEORY				EXPERIMENT		
$\tilde{\nu}$ (cm^{-1})	A km/mol	I_{rel}	Γ	$\tilde{\nu}$ (cm^{-1})	A km/mol	I_{rel}	$\tilde{\nu}$ (cm^{-1})	A km/mol	I_{rel}	Γ	$\tilde{\nu}$ (cm^{-1})	A km/mol	I_{rel}	$\tilde{\nu}$ (cm^{-1})	A km/mol	I_{rel}	Γ	$\tilde{\nu}$ (cm^{-1})	A km/mol	I_{rel}
234.1	7.1	0.114	A"				423.4	6.1	0.095	A"				240.2	5.5	0.106	A"			
477.8	12.7	0.203	A'				564.1	6.5	0.101	A"	563.3	11.5	0.18	491.0	7.3	0.142	A'			
576.9	0.6	0.010	A'	576.2	8.3	0.19	565.2	3.2	0.051	A'				672.6	3.3	0.064	A'	675.4	6.6	0.16
584.1	5.7	0.092	A"				699.9	18.7	0.292	A'	699.6*	23.1	0.37	683.8	8.2	0.159	A'	683.0	5.0	0.12
671.7	3.1	0.050	A'	674.9 677.1	5.2	0.12	754.1	55.1	0.864	A"	752.3	62.6	1.00	755.3	27.0	0.525	A"	753.2	26.7	0.64
682.6	1.4	0.023	A"				786.0	6.1	0.096	A"	787.6	5.6	0.09	781.5	51.5	1.000	A"	778.0	41.6	1.00
751.4	20.7	0.331	A"	747.5	23.5	0.54	806.3	6.0	0.095	A"	804.3	14.8	0.24	815.5	36.6	0.710	A"	805.9	9.9	0.24
783.3	27.8	0.445	A"	782.4*	35.6	0.82	825.6	65.8	1.000	A	819.9*	55.0	0.88	837.2	18.9	0.366	A"	830.2	17.6	0.42
801.8	62.5	1.000	A"	797.1*	43.7	1.0	840.7	7.1	0.111	A"	839.9	1.3	0.02	851.4	7.3	0.141	A'	843.4	6.2	0.15
837.2	12.0	0.192	A"	832.7	8.5	0.19	848.8	9.2	0.144	A'	856.3 857.8	8.2	0.13	861.9	7.7	0.150	A"	856.8	4.7	0.11
847.8	22.9	0.367	A"	837.4*	19.3	0.44	867.8	6.4	0.100	A"	864.3	5.6	0.09	871.6	12.2	0.238	A"	866.0	5.5	0.13
855.8	2.2	0.035	A'	863.8*	7.0	0.16	1020.1	10.6	0.167	A'	1028.3*	10.9	0.17	1072.2	3.6	0.069	A'	1081.4	4.0	0.10
867.4	4.6	0.073	A"				1030.1	1.9	0.030	A'				1163.6	7.5	0.146	A'	1153.9	2.3	0.06
875.9	1.2	0.018	A'				1043.4	0.6	0.009	A'	1049.8 1051.3	6.6	0.11	1176.9	1.8	0.035	A'	1163.8, 1167.7	4.8	0.12
1139.8	1.9	0.030	A'	1136.7	4.5	0.10	1264.5	19.9	0.312	A'	1268.9*	26.0	0.42	1190.4	3.3	0.064	A'	1186.9	4.0	0.10
1227.7	0.3	0.005	A'	1233.6	5.1	0.12	1384.2	8.2	0.128	A'	1401.8*	15.8	0.25	1266.1	9.1	0.177	A'	1257.4	4.2	0.10
1237.3	3.4	0.055	A'	1240.7	5.5	0.13	1428.6	10.3	0.161	A'	1439.8	13.8	0.22					1266.0	3.1	0.07
1247.2	2.4	0.038	A'	1248.2	4.5	0.10	1434.5	3.1	0.049	A'				1307.2	3.4	0.065	A'	1311.8	5.8	0.14
				1255.5	6.4	0.15	1471.4	24.1	0.377	A'	1480.7	17.8	0.28	1375.7	13.4	0.261	A'	1394.3	9.2	0.22
1259.4	11.2	0.179	A'	1263.8	7.0	0.16	1547.6	6.1	0.096	A'	1572.9	2.6	0.042	1393.3	36.3	0.704	A'	1408.0	31.9	0.77
1293.6	3.9	0.062	A'	1297.7*	8.3	0.19	1562.5	27.5	0.431	A'	1579.8	10.2	0.163	1427.3	5.2	0.100	A'	1428.9*	6.9	0.17
1351.8	9.6	0.154	A'	1380.2*	5.9	0.14	1589.2	17.8	0.278	A'	1586.4	7.6	0.121	1480.0	12.3	0.238	A'	1487.6	14.0	0.34
1400.0	14.6	0.233	A'	1410.3	12.9	0.30	1603.0	5.9	0.092	A'	1604.4	9.9	0.16	1490.5	11.6	0.226	A'	1506.5, 1510.0	7.8	0.19
1418.9	7.1	0.114	A'	1430.5*	8.5	0.19								1542.1	7.3	0.141	A'	1532.4	0.3	0.01
1434.9	3.9	0.062	A'	1438.1	4.5	0.10								1580.2	14.2	0.275	A'	1579.1	4.0	0.10
1478.6	30.3	0.485	A'	1489.4	34.4	0.79								1585.3	18.3	0.355	A'	1599.4	23.0	0.55
1504.7	9.2	0.148	A'	1518.7*	14.4	0.33														
1518.3	1.5	0.024	A'																	
1568.0	10.9	0.174	A'	1580.4	0.8	0.02														
3050.9, 3051.5, 3059.0, 3073.0, 3075.1, 3081.3, 3086.2, 3099.4*, 3105.9				3045.4, 3065.7, 3077.5*, 3093.8			3036.5, 3053.2, 3054.9, 3060.0, 3068.5, 3076.5, 3087.0, 3102.3, 3104.1				2968, 3005, 3037*, 3062*, 3103*			3049.3, 3050.5, 3052.3, 3056.5, 3057.8, 3073.6, 3083.4, 3086.0, 3098.3, 3107.3				3003, 3030, 3034, 3060*, 3072, 3090, 3105		
SUM	196.7	3.15	A'	SUM	57.5	1.30	SUM	205.6	3.73	A'	SUM	92.3	1.47	SUM	215.0	4.17	A'	SUM	83.7	2.01

[a] - data truncated at the 10% relative intensity level. The complete, untruncated tables are available electronically at www.astrochemistry.org/pahdata/index.html.

* - indicates strongest member(s) of a multiplet.

Table 2. Theoretical and experimental band positions and intensities for the neutral azabenz[a]anthracenes.[a]

1-azabenz[a]anthracene							2-azabenz[a]anthracene						
THEORY				EXPERIMENT			THEORY				EXPERIMENT		
$\tilde{\nu}$ (cm^{-1})	A km/mol	I_{rel}	Γ	$\tilde{\nu}$ (cm^{-1})	A km/mol	I_{rel}	$\tilde{\nu}$ (cm^{-1})	A km/mol	I_{rel}	Γ	$\tilde{\nu}$ (cm^{-1})	A km/mol	I_{rel}
477.0	11.6	0.222	A"				469.1	11.3	0.172	A"			
579.6	7.3	0.139	A'	576.3	8.6	0.16	519.3	6.7	0.103	A"	513.9	10.4	0.15
649.9	4.2	0.080	A'	646.3	6.9	0.13	582.4	9.5	0.144	A"	576.1	11.4	0.17
701.6	10.1	0.194	A"	694.4	11.3	0.21	744.2	40.5	0.616	A"	741.3*	49.6	0.74
745.4	32.3	0.618	A"	741.4	34.1	0.63	759.2	7.9	0.120	A'	767.9	8.1	0.12
776.3	20.5	0.392	A"	773.2	21.6	0.40	845.0	12.7	0.194	A"	838.3	12.2	0.18
816.7	30.6	0.585	A"	804.0	23.7	0.44	852.1	13.2	0.201	A"	845.1	15.9	0.24
847.4	3.4	0.064	A"	825.8	9.0	0.17	874.5	2.3	0.035	A'	883.7*	67.3	1.00
874.6	5.8	0.110	A'				889.0	65.7	1.000	A"			
895.0	42.7	0.817	A"	884.4	41.6	0.77	1221.4	8.3	0.126	A'	1226.1	2.4	0.04
937.2	1.6	0.031	A"	914.3	13.2	0.24	1239.2	14.7	0.224	A'	1239.7*	25.8	0.38
962.8	10.6	0.202	A"	954.1	5.6	0.10	1431.1	12.6	0.192	A'	1434.2	1.8	0.03
1154.5	5.2	0.100	A'	1133.6	7.4	0.14	1446.3	7.3	0.111	A'	1447.7, 1451.0	16.5	0.24
1164.2	10.4	0.200	A'	1150.3	10.3	0.19	1480.8	7.7	0.117	A'	1496.1	2.2	0.03
1273.8	6.4	0.122	A'	1269.6	5.3	0.10	1565.8	31.0	0.472	A'	1586.4	1.6	0.02
1284.1	5.3	0.102	A'	1287.4	2.6	0.05	1588.5	6.3	0.096	A'			
1305.4	2.3	0.043	A'	1310.5	5.2	0.10	1609.8	3.8	0.058	A'	1606.0*	20.3	0.3[b]
1396.6	52.3	1.000	A'	1415.9	54.2	1.00	1617.1	6.4	0.097	A'			
1414.3	1.1	0.021	A'										
1432.9	17.0	0.324	A'	1440.9	14.7	0.27							
1444.0	1.2	0.023	A'	1451.2	5.3	0.10							
1481.7	14.1	0.269	A'	1493.5	10.7	0.20							
1518.5	22.0	0.421	A'	1543.4	21.6	0.40							
1567.3	9.1	0.174	A'	1563.8	6.0	0.11							
1610.0	7.5	0.143	A'	1601.7	4.4	0.08							
3046.7, 3051.9, 3056.2, 3065.3, 3065.6, 3079.8, 3086.9				2995, 3018, 3052*, 3059*, 3067*, 3089			3048.0, 3062.6, 3066.3, 3068.6, 3077.5, 3081.0, 3082.1				2984, 3072*		
SUM	211.6	4.04	A'	SUM	132.2	2.44	SUM	207.7	3.16	A'	SUM	86.0	1.28

[a] - data truncated at the 10% relative intensity level. The complete, untruncated tables are available electronically at www.astrochemistry.org/pahdata/index.html.

[b] - Area uncertain due to overlap with band of argon matrix isolated H_2O.

* - indicates strongest member of a multiplet.

Table 3. Theoretical and experimental band positions and intensities for neutral 7,8-benzoquinoline and 2-azapyrene.[a]

7,8-benzoquinoline							2-azapyrene						
THEORY				EXPERIMENT			THEORY				EXPERIMENT		
$\tilde{\nu}$ (cm^{-1})	A km/mol	I_{rel}	Γ	$\tilde{\nu}$ (cm^{-1})	A km/mol	I_{rel}	$\tilde{\nu}$ (cm^{-1})	A km/mol	I_{rel}	Γ	$\tilde{\nu}$ (cm^{-1})	A km/mol	I_{rel}
626.1	6.2	0.121	A'	618.6, 619.9	5.0	0.11	716.7	36.4	0.712	B_1	717.6*	44.2	1.00
731.1	8.5	0.166	A"	722.3	14.0	0.30	797.8	7.8	0.153	A_1	804.7	6.3	0.14
749.4	51.2	1.000	A"	745.9*	46.5	1.00	807.0	11.5	0.224	B_1	816.5	21.0	0.48
821.1	41.8	0.817	A"	807.6	16.6	0.36	819.8	4.9	0.096	A_1	822.4*	9.2	0.21
				825.6	9.1	0.20	839.6	51.1	1.000	B_1	846.8*	21.7	0.49
852.6	26.5	0.517	A"	834.0*	35.3	0.76	904.9	41.4	0.810	B_1	893.7*	25.2	0.57
942.7	0.9	0.018	A"	953.9*	7.0	0.15					1024.9	5.7	0.13
964.1	2.2	0.043	A"				1077.8	3.5	0.068	A_1	1077.1	5.2	0.12
1013.9	4.5	0.088	A'	1018.2	4.6	0.10	1123.8	7.7	0.151	A_1	1142.1, 1143.3	13.9	0.31
1084.3	4.2	0.081	A'	1095.2	4.9	0.10	1187.8	6.2	0.122	B_2	1180.2, 1183.0	8.2	0.19
1141.2	0.6	0.013	A'	1133.4	5.1	0.11	1210.7	4.6	0.090	B_2	1208.0	6.6	0.15
1388.9	35.0	0.683	A'	1405.7*	23.9	0.52	1245.8	0.9	0.018	A_1	1239.4	10.4	0.24
1439.1	13.4	0.262	A'	1447.7*	19.3	0.42	1259.2	4.2	0.083	A_1	1254.4*	8.9	0.20
1445.8	9.1	0.178	A'				1382.1	6.8	0.132	B_2	1385.0	4.2	0.09
1489.8	6.1	0.120	A'	1500.4	8.6	0.18	1425.2	3.8	0.075	B_2	1422.7	1.3	0.17
1499.4	15.4	0.300	A'	1515.5*	7.6	0.16	1429.8	14.8	0.289	A_1	1427.5	0.03	0.004
1575.4	12.3	0.239	A'	1574.1, 1575.3	4.7	0.10	1439.1	6.1	0.120	A_1	1433.3*	3.7	0.08
1597.2	4.2	0.083	A'	1595.2	15.2	0.33					1460.5*	9.2	0.21
							1561.2	5.2	0.101	B_2	1542.9*	8.0	0.18
							1588.7	11.3	0.222	B_2	1572.9	3.7	0.08
3049.8, 3055.3, 3059.4, 3065.2, 3076.1, 3086.7, 3102.6				2932, 2965, 3034, 3060*, 3099			3045.2, 3052.0, 3058.4, 3068.1, 3077.4				3012, 3018, 3029, 3042*, 3051, 3057		
SUM	173.3	3.38	A'	SUM	88.2	1.90	SUM	173.3	3.39	A_1, B_2	SUM	67.5	1.53

[a] - data truncated at the 10% relative intensity level. The complete, untruncated tables are available electronically at www.astrochemistry.org/pahdata/index.html.

* - indicates strongest member of a multiplet.

Table 4. A comparison of the total absolute absorption intensities of PANHs to their parent PAHs in the 1100 - 500 cm^{-1}, 1600 - 1100 cm^{-1}, and 3150 - 2950 cm^{-1} regions of the spectrum.

	EXPERIMENT			THEORY		
	$\sum A_{1100>\tilde{\nu}>500}$	$\sum A_{1600>\tilde{\nu}>1100}$	$\sum A_{3150>\tilde{\nu}>2950}$	$\sum A_{1100>\tilde{\nu}>500}$	$\sum A_{1600>\tilde{\nu}>1100}$	$\sum A_{3150>\tilde{\nu}>2950}$ †
PAHs	*(km/mol)*	*(km/mol)*	*(km/mol)*	*(km/mol)*	*(km/mol)*	*(km/mol)*
phenanthrene	176	48	126	167	52	199
pyrene	186	54	102	176	58	217
benz[a]anthracene	203	65	120	204	69	242
chrysene	217	63	126	210	70	236
PANHs	*(km/mol)*	*(km/mol)*	*(km/mol)*	*(km/mol)*	*(km/mol)*	*(km/mol)*
7,8-benzoquinoline	164	113	88	166	126	177
2-azapyrene	157	100	76	171	102	181
1-azabenz[a]anthracene	197	165	132	193	176	221
2-azabenz[a]anthracene	209	123	86	194	142	218
1-azachrysene	181	136	57	198	130	202
2-azachrysene	218	128	92	210	152	207
4-azachrysene	150	135	84	206	160	216
Ratios						
7,8-benzoquinoline/phenanthrene	0.93	2.37	0.70	0.99	2.39	0.89
2-azapyrene/pyrene	0.84	1.86	0.74	0.97	1.76	0.83
1-azabenz[a]anth./benz[a]anth.	0.97	2.53	1.10	0.95	2.55	0.91
2-azabenz[a]anth./benz[a]anth.	1.03	1.88	0.71	0.95	2.05	0.90
1-azachrysene/chrysene	0.83	2.17	0.45	0.94	1.85	0.86
2-azachrysene/chrysene	1.01	2.03	0.73	1.00	2.16	0.88
4-azachrysene/chrysene	0.69	2.14	0.66	0.98	2.28	0.92
Average	0.90	2.14	0.73	0.97	2.15	0.88

† - the theoretical CH stretching intensities are not corrected for the expected factor of ≈2 overestimate associated with calculations at the B3LYP/4-31G level (see §II.B).[3a]

Table 5. A comparison of the average Mulliken populations on the carbon atoms of several PANHs and their corresponding parent aromatic hydrocarbons.

Molecule	Average Mulliken Population on Skeletal Carbon Atoms	
	Neutral	Cation
phenanthrene	-0.091	-0.066
7,8-benzoquinoline	-0.058	-0.029
pyrene	-0.080	-0.057
2-azapyrene	-0.054	-0.028
benz[a]anthracene	-0.086	-0.065
1-azabenz[a]anthracene	-0.060	-0.037
2-azabenz[a]anthracene	-0.063	-0.042
chrysene	-0.086	-0.066
1-azachrysene	-0.060	-0.039
2-azachrysene	-0.064	-0.042
4-azachrysene	-0.060	-0.037

Table 6. Theoretical and experimental band positions and intensities for the azachrysene cations.[a]

1-azachrysene						2-azachrysene						4-azachrysene					
THEORY				EXPERIMENT		THEORY				EXPERIMENT		THEORY				EXPERIMENT	
$\tilde{\nu}$ (cm^{-1})	A km/mol	I_{rel}	Γ	$\tilde{\nu}$ (cm^{-1})	I_{rel}	$\tilde{\nu}$ (cm^{-1})	A km/mol	I_{rel}	Γ	$\tilde{\nu}$ (cm^{-1})	I_{rel}	$\tilde{\nu}$ (cm^{-1})	A km/mol	I_{rel}	Γ	$\tilde{\nu}$ (cm^{-1})	I_{rel}
543.6	3.5	0.012	A'	547.1	0.44	757.3	39.7	0.106	A"	750.6	0.06	561.1	20.9	0.064	A'	552.6	0.20
757.0	34.9	0.117	A"	752.6	0.07	820.7	40.2	0.107	A"			758.9	53.3	0.162	A"		
778.0	16.7	0.056	A"	781.4	0.10	1093.3	61.7	0.165	A'	1098.7	0.31	1151.9	83.2	0.253	A'	1139.0	0.68
811.3	52.0	0.174	A"	806.5	0.08	1139.0	64.2	0.172	A'			1218.5	57.6	0.175	A'		
858.3	42.8	0.143	A"			1178.3	40.9	0.109	A'			1232.7	101.4	0.309	A'		
1037.4	42.7	0.143	A'	1046.1*	0.14	1229.7	296.8	0.794	A'	1233.6	0.57	1248.3	9.6	0.029	A'	1258.9	0.17
1053.1	28.6	0.096	A'	1060.9	0.12	1249.1	42.2	0.113	A'			1273.7	3.1	0.009	A'	1276.4	0.14
1130.9	43.5	0.146	A'	1130.0	0.32	1290.2	159.4	0.427	A'	1293.3*	1.00	1287.4	328.4	1.000	A'	1297.9*	1.00
1150.6	24.6	0.082	A'	1148.7	0.11	1305.2	15.8	0.042	A'			1326.6	92.9	0.283	A'	1327.6	0.26
1188.3	18.2	0.061	A'	1178.9*	0.10	1315.7	20.8	0.056	A'			1341.1	39.9	0.122	A'		
1230.8	107.8	0.361	A'	1231.9	0.62	1339.9	219.7	0.588	A'			1367.1	53.5	0.163	A'		
1237.7	58.5	0.196	A'			1425.5	61.8	0.165	A'	1430.4	0.23	1420.7	40.8	0.124	A'		
1286.0	23.8	0.080	A'	1285.0	0.11	1440.2	47.1	0.126	A'	1446.2*	0.47	1467.8	232.1	0.707	A'	1482.0*	0.78
1301.2	73.5	0.246	A'	1310.5	0.19	1492.6	110.3	0.295	A'	1481.9	0.04	1487.3	114.5	0.349	A'		
1339.5	211.3	0.707	A'	1338.7	0.45	1512.3	256.2	0.686	A'			1530.4	234.1	0.713	A'		
1353.4	42.4	0.142	A'	1351.0	0.09	1528.7	373.7	1.000	A'	1553.0*	0.65	1542.3	139.5	0.425	A'	1564.4	0.43
1419.4	78.4	0.262	A'	1431.7	0.17	1539.8	54.0	0.144	A'			1552.6	109.1	0.332	A'	1579.3	0.23
1438.2	15.5	0.052	A'	1437.5*	0.36	1551.1	222.9	0.596	A'	1575.5	0.20	1576.7	12.6	0.039	A'		
1479.7	298.9	1.000	A'	1478.7	0.19												
1485.2	10.3	0.035	A'	1487.1	1.00												
1501.9	125.5	0.420	A'	1494.1	0.03												
1515.6	81.6	0.273	A'	1509.3	0.17												
1529.6	101.2	0.339	A'														
1544.4	151.0	0.505	A'	1558.7*	0.49												
3086.5, 3093.3, 3102.3, 3106.6, 3107.9, 3115.0, 3120.6						3066.5, 3104.4, 3106.5, 3116.9						3087.1, 3105.9, 3108.8, 3109.7, 3114.2					
SUM	34.0	0.114	A'			SUM	25.5	0.068	A'			SUM	28.6	0.087	A'		

[a] - data for $\tilde{\nu}$<1600 cm^{-1} truncated at the 10% relative intensity level; data for 3120< $\tilde{\nu}$<3000 cm^{-1} truncated at the 1% relative intensity level. The complete, untruncated tables are available electronically at www.astrochemistry.org/pahdata/index.html.

* - indicates strongest member of a multiplet.

Table 7. Theoretical and experimental band positions and intensities for the azabenz[a]anthracene cations.[a]

1-azabenz[a]anthracene						2-azabenz[a]anthracene					
THEORY				EXPERIMENT		THEORY				EXPERIMENT	
$\tilde{\nu}$ (cm^{-1})	A km/mol	I_{rel}	Γ	$\tilde{\nu}$ (cm^{-1})	I_{rel}	$\tilde{\nu}$ (cm^{-1})	A km/mol	I_{rel}	Γ	$\tilde{\nu}$ (cm^{-1})	I_{rel}
756.9	45.1	0.114	A"	752.1	0.03	668.6	6.9	0.029	A'	664.0	0.12
774.9	21.0	0.053	A"			755.7	48.5	0.206	A"		
820.0	26.1	0.066	A"	803.4	0.06	854.2	28.2	0.120	A"	848.9	0.07
918.6	29.6	0.075	A"	915.6	0.03	912.2	40.1	0.170	A"		
1156.0	28.5	0.072	A'	1146.4	0.07	1192.3	33.1	0.140	A'	1184.1	0.11
1186.8	0.6	0.002	A'	1182.9	0.08	1222.6	42.6	0.181	A'	1213.6	0.16
1190.3	27.4	0.069	A'	1192.7	0.05	1236.7	187.1	0.793	A'	1230.8	1.00
1208.9	89.0	0.225	A'	1212.8*	0.14	1332.8	219.7	0.931	A'	1347.6	0.44
1233.1	37.9	0.096	A'	1229.1	0.02	1352.4	236.0	1.000	A'	1361.8	0.22
1308.7	130.5	0.330	A'	1317.6	0.13	1364.7	142.6	0.604	A'	1367.3	0.39
				1325.5*	0.12	1402.2	11.2	0.048	A'	1380.8	0.13
1336.2	395.4	1.000	A'	1340.2	1.00	1463.8	46.8	0.198	A'	1478.7	0.08
1352.6	28.2	0.071	A'	1354.4	0.02	1474.4	39.6	0.168	A'		
				1358.2	0.05	1483.8	29.0	0.123	A'		
				1365.5	0.08	1508.6	48.1	0.204	A'	1513.3	0.27
1370.0	128.0	0.324	A'	1391.6	0.38	1530.0	74.4	0.315	A'	1531.3	0.24
1389.4	67.5	0.171	A'	1411.8	0.18	1540.5	43.9	0.186	A'	1547.9	0.15
1433.7	12.4	0.031	A'	1428.0	0.05	1556.9	47.1	0.199	A'		
1471.2	82.5	0.209	A'	1478.0	0.04	1564.5	24.6	0.104	A'		
1488.2	31.1	0.079	A'								
1511.9	17.6	0.044	A'	1511.9	0.06						
1530.2	93.2	0.236	A'	1537.7	0.12						
1543.6	32.3	0.082	A'	1551.4	0.04						
1559.5	62.3	0.158	A'	1570.7	0.06						
1573.9	50.3	0.127	A'	1583.3	0.05						
				1599.7	0.05						
3083.1, 3087.6, 3091.2, 3105.0, 3107.1						3075.4, 3089.5, 3096.0, 3105.9, 3108.2					
SUM	30.3	0.077	A'			SUM	30.0	0.127	A'		

[a] - data for $\tilde{\nu}$<1600 cm^{-1} truncated at the 10% relative intensity level; data for 3120< $\tilde{\nu}$<3000 cm^{-1} truncated at the 1% relative intensity level. The complete, untruncated tables are available electronically at www.astrochemistry.org/pahdata/index.html.

* - indicates strongest member of a multiplet.

Table 8. Theoretical and experimental band positions and intensities for the 7,8-benzoquinoline and 2-azapyrene cations.[a]

7,8-benzoquinoline						2-azapyrene					
THEORY				EXPERIMENT		THEORY				EXPERIMENT	
$\tilde{\nu}$ (cm^{-1})	A km/mol	I_{rel}	Γ	$\tilde{\nu}$ (cm^{-1})	I_{rel}	$\tilde{\nu}$ (cm^{-1})	A km/mol	I_{rel}	Γ	$\tilde{\nu}$ (cm^{-1})	I_{rel}
543.7	17.0	0.137	A'	536.3	0.36	689.3	41.7	0.205	B_1	694.8	0.15
606.5	8.8	0.071	A'	596.6	0.14	847.5	60.1	0.295	B_1	855.8	0.09
700.9	41.5	0.335	A"	698.2	0.36	918.8	35.7	0.175	B_1	914.1	0.07
757.7	29.5	0.238	A"			978.0	24.8	0.122	B_2	990.7	0.11
817.8	22.5	0.181	A"			992.4	50.4	0.247	A_1	1004.8	0.10
863.1	36.9	0.298	A"	853.5	0.20	1254.7	77.9	0.382	A_1	1259.2	0.13
863.4	15.4	0.124	A'	870.6	0.12	1275.6	23.2	0.114	B_2	1305.1*	0.70
999.2	43.2	0.349	A'	1003.1	0.20	1337.7	111.6	0.547	B_2	1351.7*	0.33
1018.4	20.7	0.167	A"	1012.2	0.11	1362.8	5.1	0.025	B_2	1358.7	0.25
1019.6	0.7	0.006	A"	1024.8	0.10	1411.7	43.0	0.211	B_2	1428.0*	0.31
1044.2	5.5	0.045	A'	1053.0	0.10	1434.4	25.8	0.127	A_1		
1113.0	16.6	0.134	A'			1451.6	30.1	0.147	A_1		
1143.6	51.1	0.413	A'	1139.9	0.22	1523.0	204.0	1.000	B_2	1548.7	1.00
1169.1	53.3	0.430	A'	1159.9*	0.60						
1205.0	43.5	0.351	A'	1202.6*	0.80						
1213.0	22.7	0.184	A'	1216.5	0.08						
1239.1	74.8	0.604	A'	1230.7	0.09						
1253.0	123.4	0.996	A'	1243.1	1.00						
				1249.8	0.16						
				1259.6	0.25						
1304.5	53.8	0.435	A'	1308.2	0.40						
1409.5	59.1	0.477	A'	1420.5	0.14						
1424.3	7.2	0.058	A'	1431.7	0.03						
1467.3	67.4	0.544	A'	1439.1	0.69						
1484.2	9.8	0.080	A'	1490.7*	0.90						
1508.3	11.6	0.094	A'	1509.0	0.12						
1517.2	123.8	1.000	A'	1536.3*	0.92						
1547.4	103.0	0.832	A'								
1574.7	63.6	0.513	A'	1583.1	0.09						
	3089.1, 3111.7						3073.7, 3090.7				
SUM	6.0	0.049	A'			SUM	6.1	0.030	B_2		

[a] - data for $\tilde{\nu}$<1600 cm^{-1} truncated at the 10% relative intensity level; data for 3120< $\tilde{\nu}$<3000 cm^{-1} truncated at the 1% relative intensity level. The complete, untruncated tables are available electronically at www.astrochemistry.org/pahdata/index.html.

* - indicates strongest member of a multiplet.

Table 9. A comparison of the total absolute absorption intensities of PANHs and their corresponding PAHs in neutral and cationic forms in the 1100 - 500 cm^{-1}, 1600 - 1100 cm^{-1}, and 3150 - 2950 cm^{-1} regions of the spectrum.

	$\sum A$ $1100>\tilde{\nu}>500$		$\sum A$ $1600>\tilde{\nu}>1100$		$\sum A$ † $3150>\tilde{\nu}>2950$		Ratios (cation/neutral)		
	neutral *km/mol*	cation *km/mol*	neutral *km/mol*	cation *km/mol*	neutral *km/mol*	cation *km/mol*	$\sum A$ $1100>\tilde{\nu}>500$	$\sum A$ $1600>\tilde{\nu}>1100$	$\sum A$ $3150>\tilde{\nu}>2950$
PAHs									
phenanthrene	167	260	52	953	199	15	1.55	18.2	0.07
pyrene	176	225	58	525	217	13	1.28	9.1	0.06
benz[a]anthracene	204	267	69	1694	242	44	1.31	24.5	0.18
chrysene	210	297	70	2064	236	49	1.41	29.4	0.21
Average							1.39	20.3	0.13
PANHs									
7,8-benzoquinoline	166	268	126	905	177	11	1.62	7.2	0.06
2-azapyrene	171	242	102	616	181	8	1.41	6.0	0.05
1-azabenz[a]anth.	193	234	176	1370	221	36	1.21	7.8	0.17
2-azabenz[a]anth.	194	205	142	1350	218	34	1.05	9.5	0.15
1-azachrysene	198	320	130	1552	202	37	1.62	12.0	0.18
2-azachrysene	210	329	152	2099	207	34	1.57	13.8	0.17
4-azachrysene	206	280	160	1762	216	36	1.36	11.0	0.17
Average							1.41	9.6	0.13

† - the theoretical CH stretching intensities are not corrected for the expected factor of ≈2 overestimate associated with calculations at the B3LYP/4-31G level (see §II.B). ref: L&B, spectrochim.acta

Table 10. Calculated dipole moments and rotational constants for several neutral and cationic PANH species.[a]

	Neutral						Cation					
PANH	μ_A (D)	A (GHz)	μ_B (D)	B (GHz)	μ_C (D)	C (GHz)	μ_A (D)	A (GHz)	μ_B (D)	B (GHz)	μ_C (D)	C (GHz)
7,8-benzoquinoline	0.7	1.609	-1.71	0.568	0	0.420	-0.68	1.626	-2.32	0.563	0	0.418
2-azapyrene	-3.16	1.019	0	0.555	0	0.359	-3.59	1.027	0	0.551	0	0.359
1-azabenz[a]anth.	0.92	1.164	1.39	0.262	0	0.214	-1.39	1.166	1.76	0.262	0	0.214
2-azabenz[a]anth.	-1.77	1.170	2.43	0.257	0	0.210	-4.61	1.173	2.88	0.256	0	0.210
1-azachrysene	1.44	1.267	1.95	0.264	0	0.218	3.11	1.279	2.2	0.261	0	0.217
2-azachrysene	3.36	1.271	0.21	0.262	0	0.217	4.34	1.283	0.36	0.259	0	0.216
4-azachrysene	-0.48	1.259	-1.82	0.268	0	0.221	1.38	1.270	-1.76	0.265	0	0.220

[a] - the (a, b, c) coordinate system s as defined in Figure1.

Figure 1.

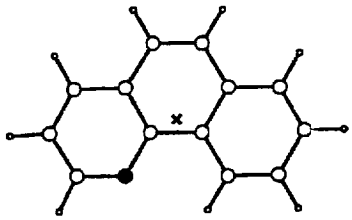

μ_0=1.85D μ_+=2.42D

7,8-benzoquinoline

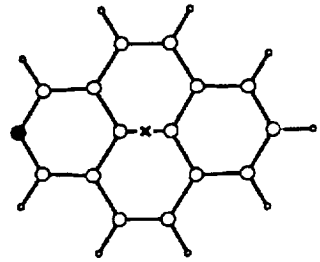

μ_0=3.16D

μ_+=3.59D

2-azapyrene

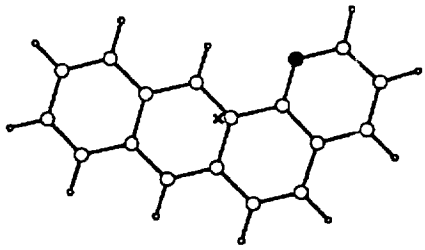

μ_+=2.24D μ_0=1.67D

1-azabenz[a]anthracene

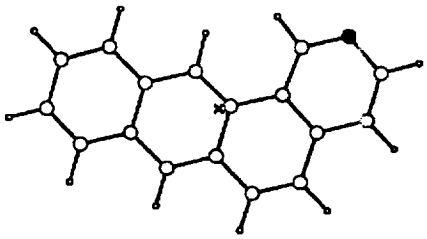

μ_+=5.44D μ_0=3.01D

2-azabenz[a]anthracene

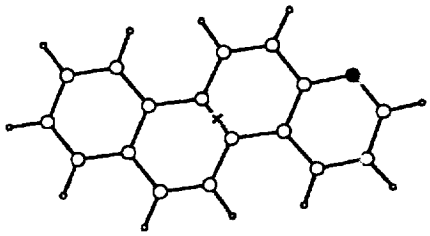

μ_+=3.81D μ_0=2.42D

1-azachrysene

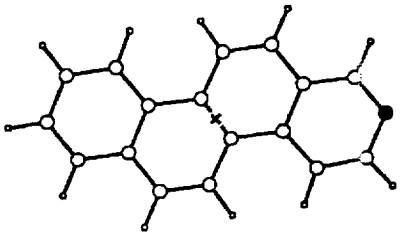

μ_+=4.35D μ_0=3.37D

2-azachrysene

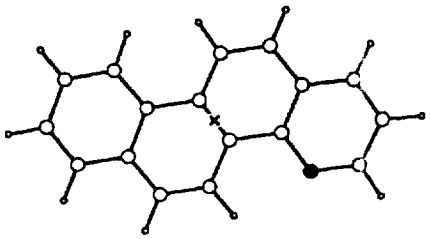

μ_+=2.24D μ_0=1.88D

4-azachrysene

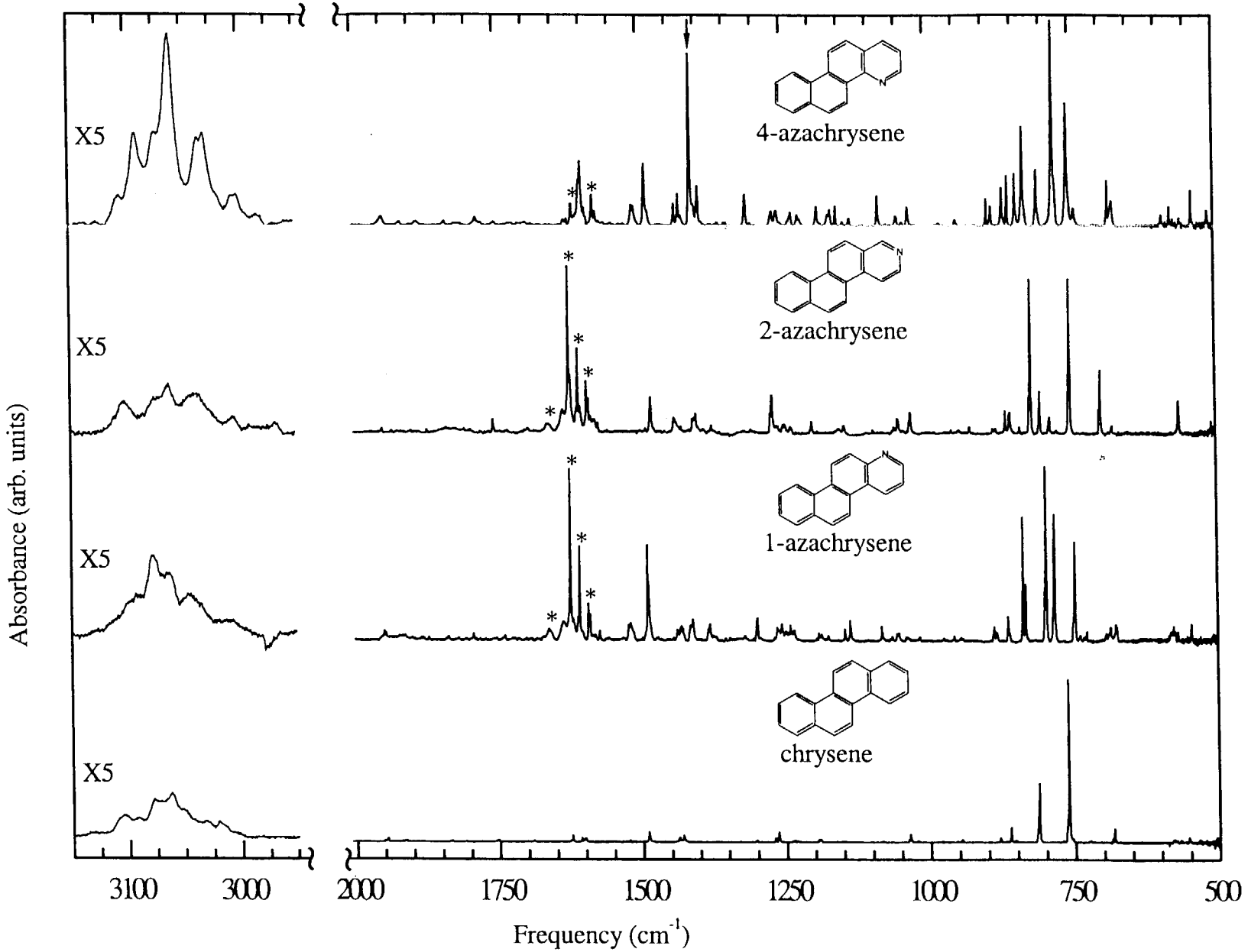
X5
X5
X5
X5
4-azachrysene
2-azachrysene
1-azachrysene
chrysene
Absorbance (arb. units)
3100
3000
2000
1750
1500
1250
1000
750
500
Frequency (cm-1)

Figure 2.

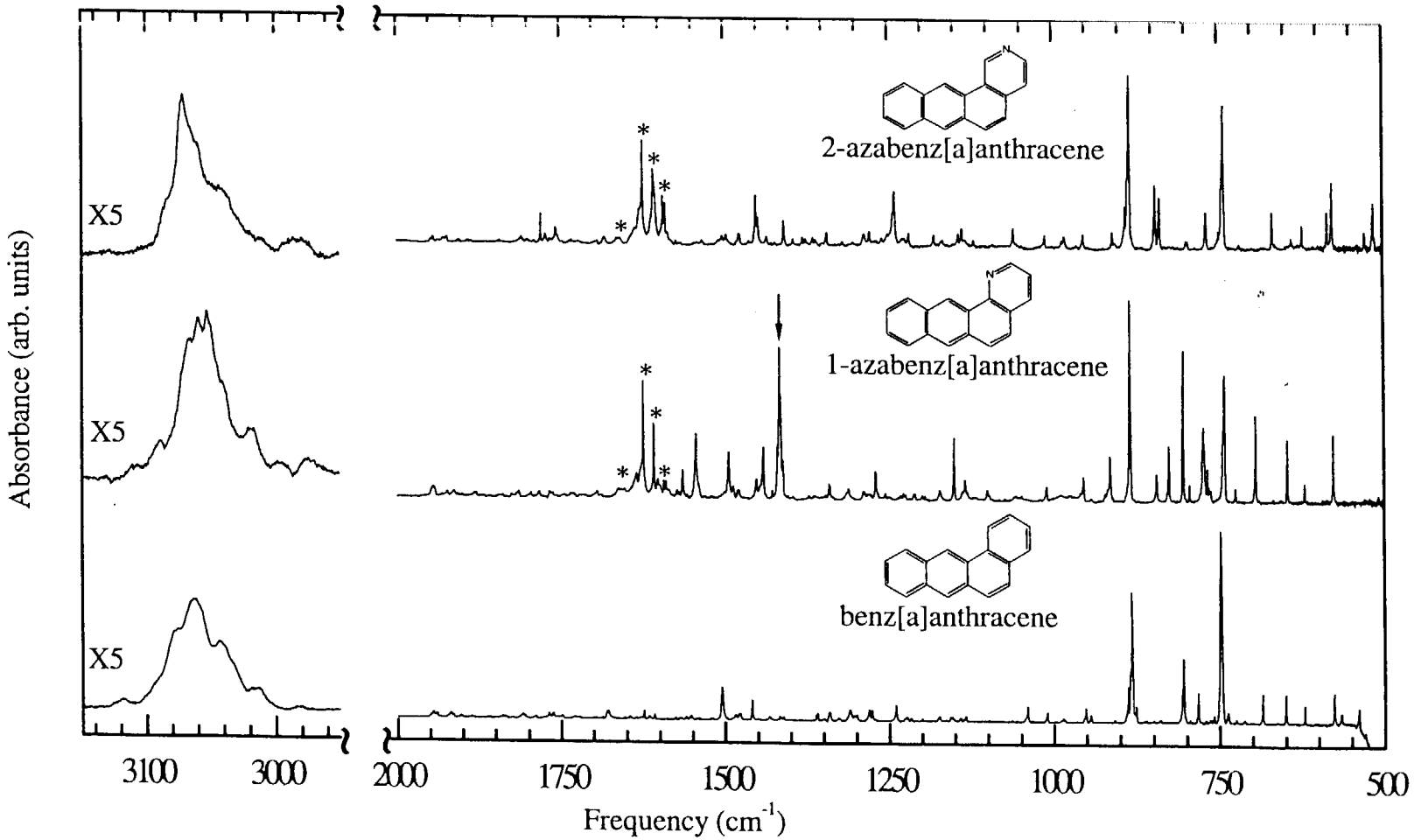
Absorbance (arb. units)
X5
X5
X5
2-azabenz[a]anthracene
1-azabenz[a]anthracene
benz[a]anthracene
3100
3000
2000
1750
1500
1250
1000
750
500
Frequency (cm-1)

Figure 3.

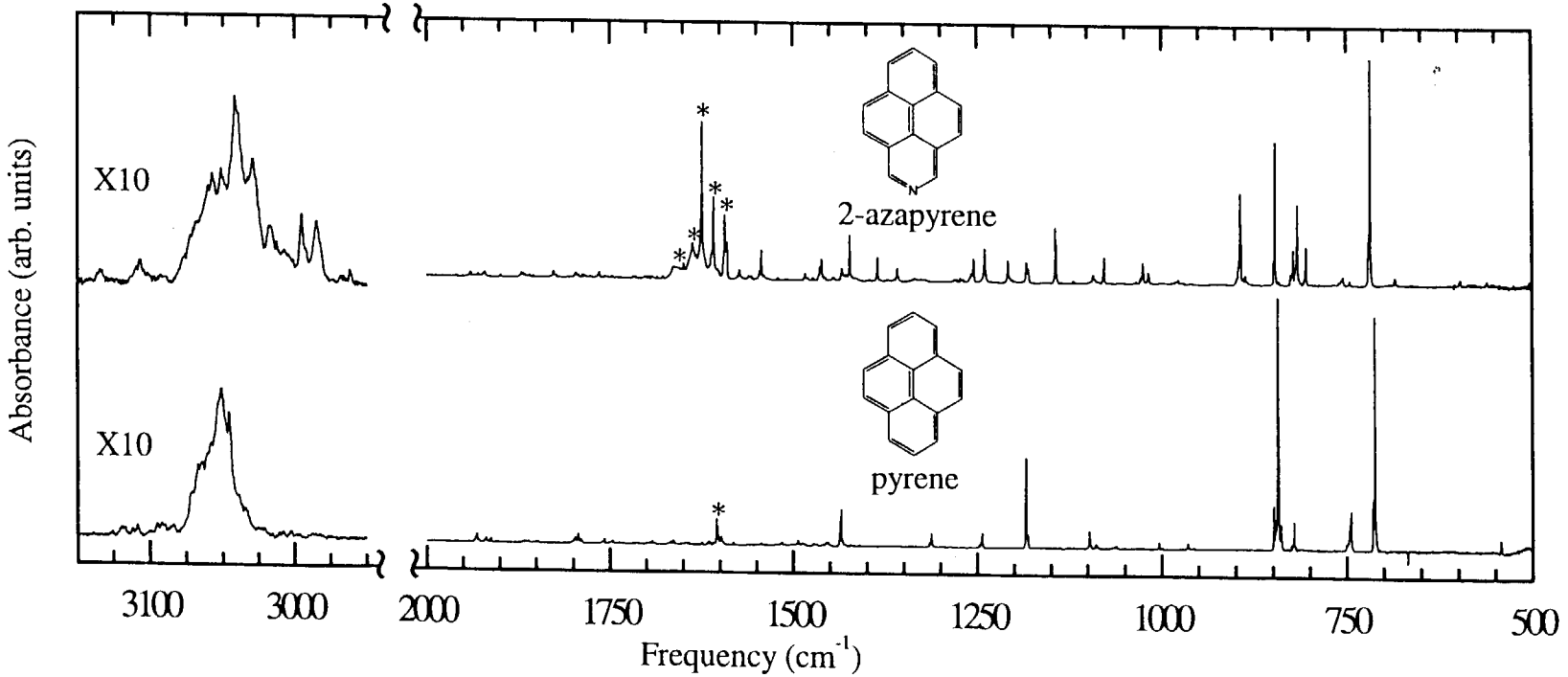
Absorbance (arb. units)
X10
X10
2-azapyrene
pyrene
3100
3000
2000
1750
1500
1250
1000
750
500
Frequency (cm-1)

Figure 4.

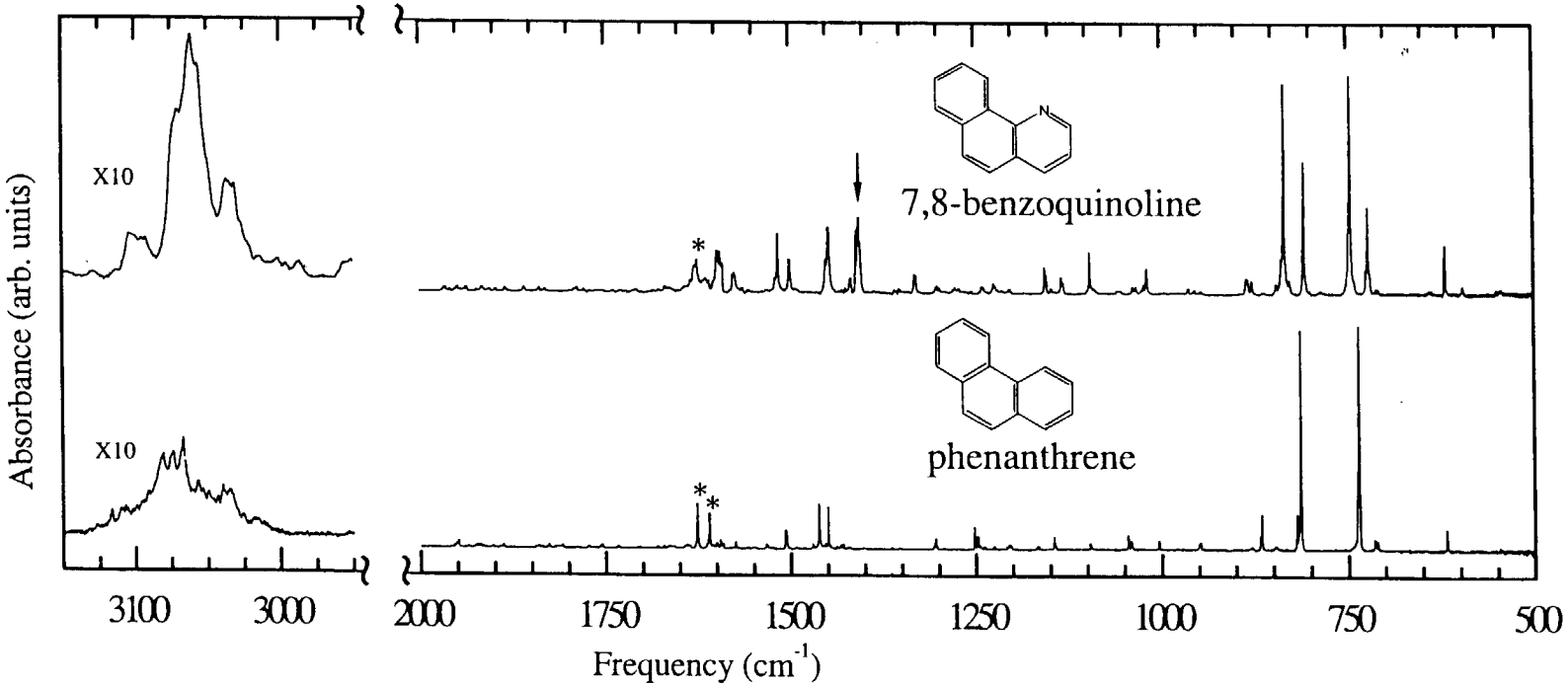
Absorbance (arb. units)
X10
X10
7,8-benzoquinoline
phenanthrene
*
*
*
3100
3000
2000
1750
1500
1250
1000
750
500
Frequency (cm-1)

Figure 5.

Figure 6.

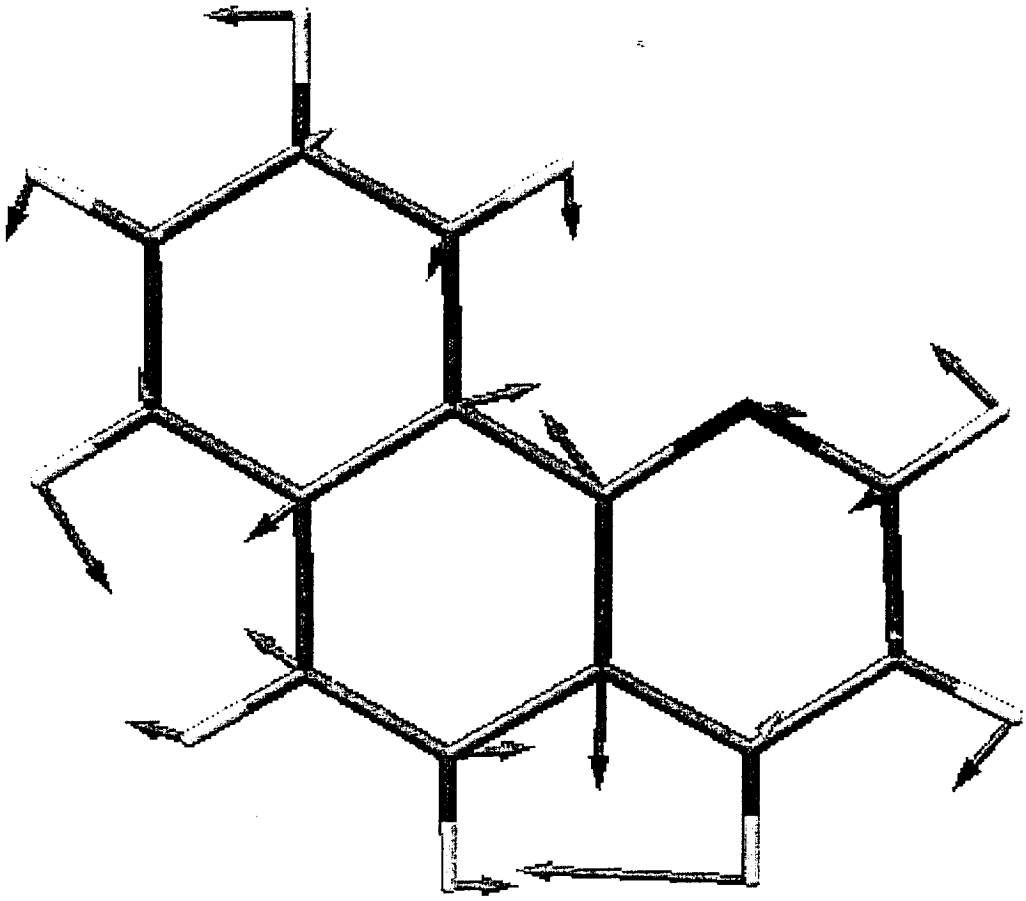

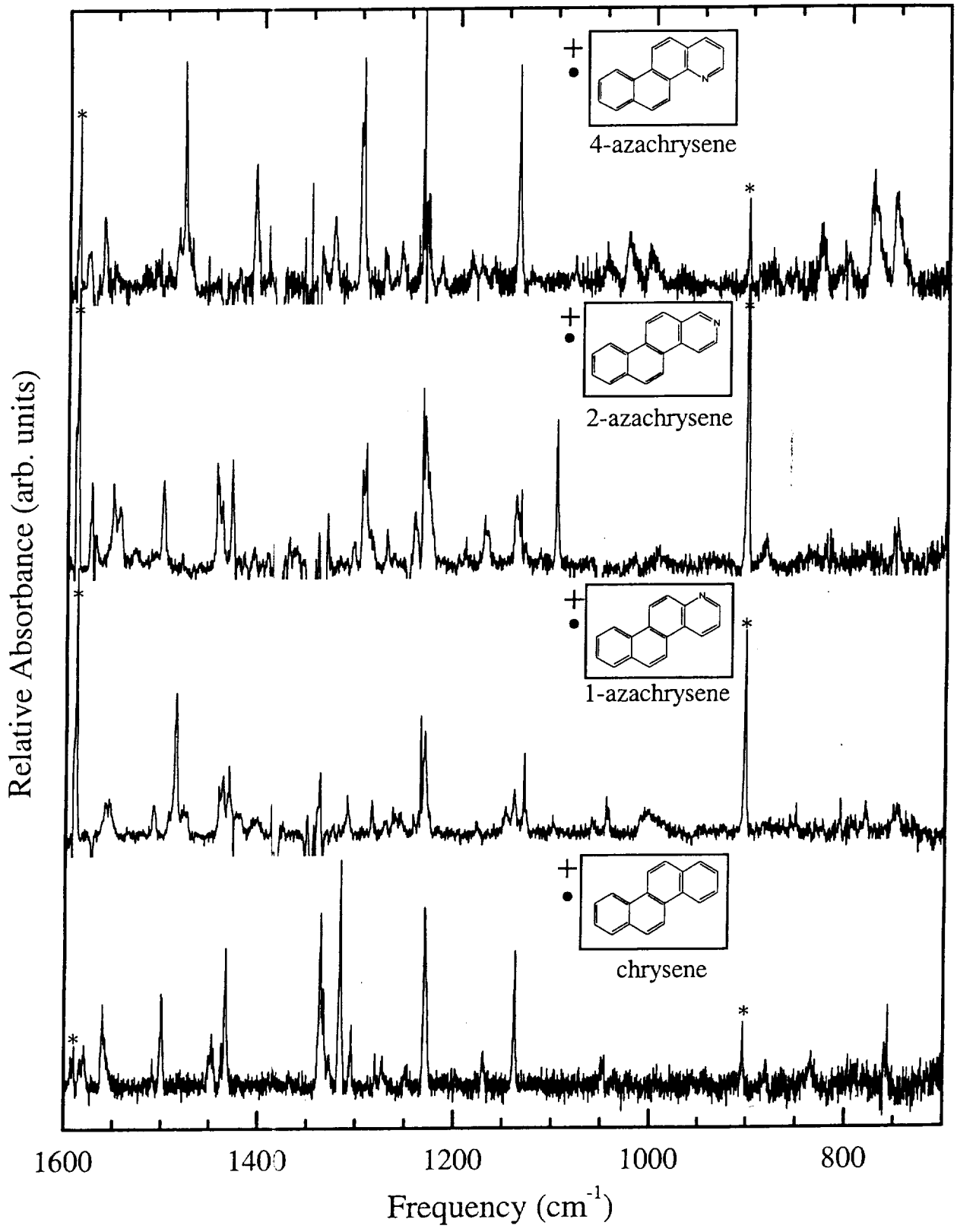
4-azachrysene
2-azachrysene
1-azachrysene
chrysene
Relative Absorbance (arb. units)
1600
1400
1200
1000
800
Frequency (cm-1)

Figure 7.

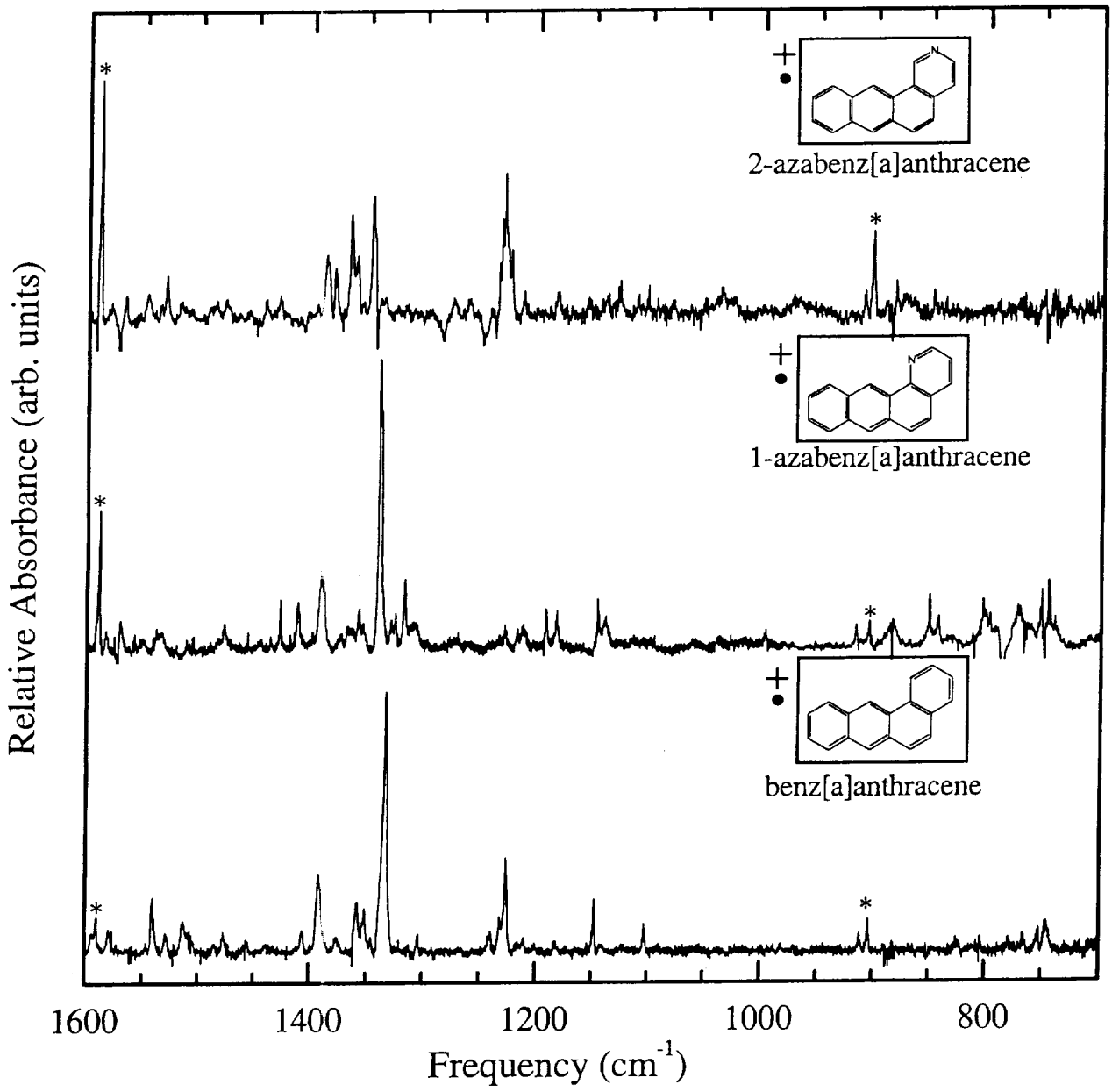
2-azabenz[a]anthracene
1-azabenz[a]anthracene
benz[a]anthracene
Relative Absorbance (arb. units)
1600
1400
1200
1000
800
Frequency (cm-1)

Figure 8.

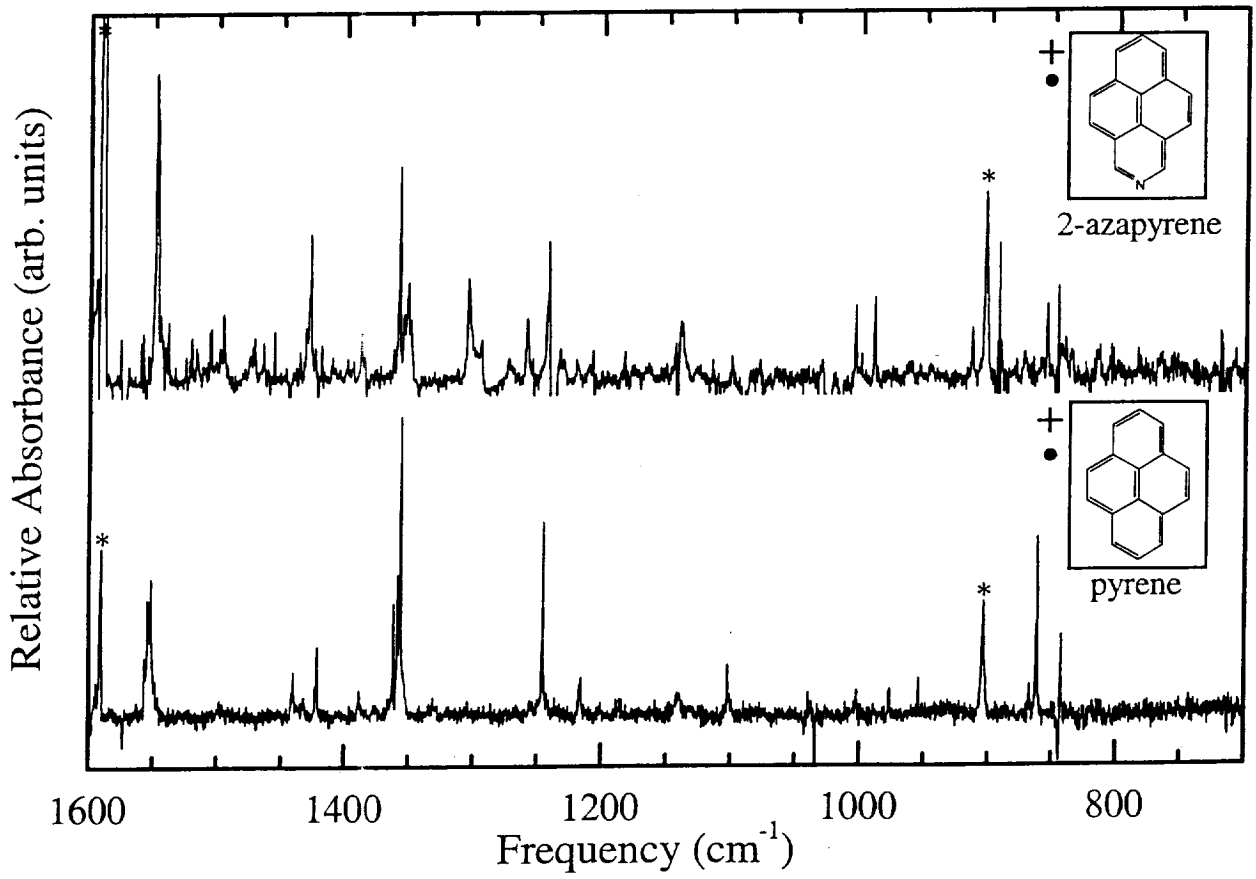
Relative Absorbance (arb. units)
1600
1400
1200
1000
800
Frequency (cm-1)
2-azapyrene
pyrene
*
*
*
*

Figure 9

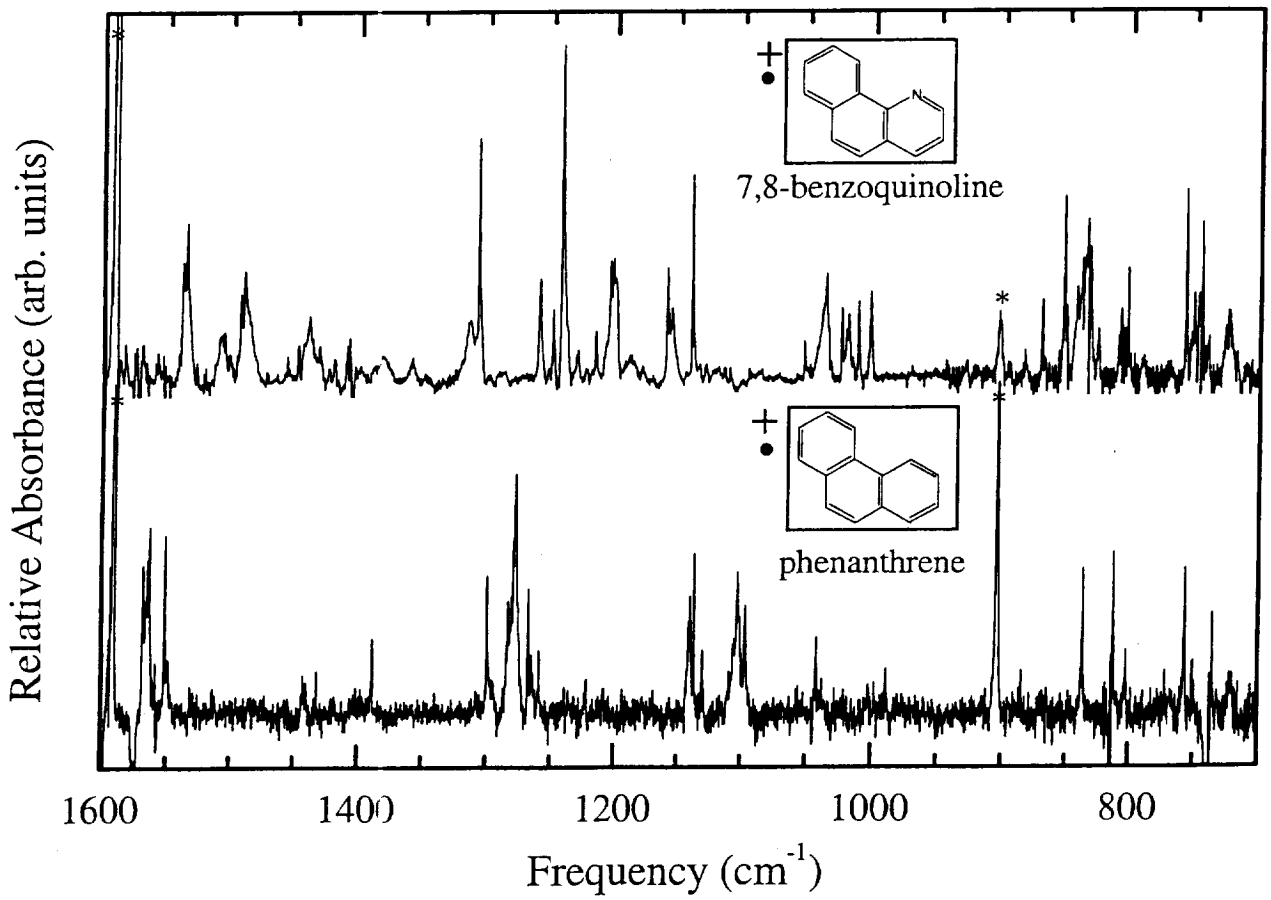
Relative Absorbance (arb. units)
7,8-benzoquinoline
phenanthrene
1600
1400
1200
1000
800
Frequency (cm-1)

Figure 10.